Energy Conversion and Management 192 (2019) 114–132

Contents lists available at ScienceDirect

Energy Conversion and Management

journal homepage: www.elsevier.com/locate/enconman

# Exergy cost and thermoeconomic analysis of a Rankine Cycle + Multi-Effect Distillation plant considering time-varying conditions

Carlos Mata-Torres[a,*], Adriana Zurita[a], José M. Cardemil[b], Rodrigo A. Escobar[a,c]

[a] Departamento de Ingeniería Mecánica y Metalúrgica, Escuela de Ingeniería, Pontificia Universidad Católica de Chile, Vicuña Mackenna 4860, Santiago, Chile
[b] Departamento de Ingeniería Mecánica, Facultad de Ciencias Físicas y Matemáticas, Universidad de Chile, Beauchef 851, Santiago, Chile
[c] Centro del Desierto de Atacama, Centro de Energía, Escuela de Ingeniería. Pontificia Universidad Católica de Chile, Vicuña Mackenna 4860, Santiago, Chile

ARTICLE INFO

*Keywords:*
Thermal desalination
MED
Cogeneration plant
Exergetic cost analysis
Thermoeconomic analysis

ABSTRACT

A detailed exergy cost and thermoeconomic analysis applied to a Rankine Cycle (RC) coupled to a Multi-Effect Distillation (MED) plant was performed. The aim of this work is to identify the impact of design and operating conditions on the exergy and thermoeconomic costs of the final products, electricity, and freshwater, and to assess the distribution of the destroyed exergy, the fuel, and the plant costs. The plant model considers a high disaggregation model, which includes MED plant and condenser parasitic losses, a seawater pumping system and a brine energy recovery system. It also considers solar molten salts as the RC fuel, which is the typical fluid used in solar tower plants. The impact of RC + MED plant part-load operation, ambient temperature, MED plant size, and location plant's altitude was evaluated and an analysis of operational day of the RC + MED plant was carried out. Results indicate that the plant part-load operation has a significant influence on the unit exergy and thermoeconomic product costs, while the ambient temperature evidences only a minor effect on the water costs. As well, the largest MED plant sizes (above 50,000 $m^3$/day) offer the lowest electric and water costs, while the altitude strongly increases the water costs.

## 1. Introduction

Freshwater is considered a renewable resource, but climate change has led to a growing water scarcity, which is particularly evident in arid regions [1]. This situation has encouraged a growing interest in desalination technologies increasing their global installed capacity in the last years [2,3]. Reverse Osmosis (RO) dominates the market accounting for almost 65% of the installed capacity, whereas the different thermal desalination technologies cover the remaining capacity [4]. In particular, the main issue of thermal desalination plants is their high-energy consumption [5], therefore, research has been focused on improving their design, energy efficiency and operation [6–9], and evaluating the integration of thermal desalination in dual purpose or cogeneration plants to produce electricity and water [10–12]. In cogeneration plants, the high-grade heat given by the fuel is transformed into electrical power, and the residual low-grade heat is used by the thermal desalination process to produce water. Moreover, most of the desalination plants are located in arid regions with high availability of solar radiation, which enables the possibility to drive water desalination processes and cogeneration plants using solar energy. These processes have received large attention from the scientific community during recent years since solar desalination offers a sustainable means of renewable energy utilization at low operational costs [5].

Recent literature shows several studies focusing on the analysis and optimization of the integration between Concentrating Solar Power (CSP) plants and Multi-Effect Distillation (MED) systems [13–18]. These studies evidence the high potential of implementation of these systems, based on their energy and techno-economic performance. In addition, these studies have shown that the integration can be even more favorable than the integration with RO, depending on the plant location, environmental conditions, among other local features. Palenzuela et al. [15,16] results showed that the CSP + MED plant presents a higher energy efficiency (around 2%) than the CSP + RO when the exhaust steam leaves the turbine at high temperatures (more than 55 °C) due to the use of air-cooled condenser, and also when the seawater presents high salinity (42 $g_{salt}/kg_{water}$), which increases the RO unit electric consumption. Nonetheless, the overall products costs of the CSP + RO plant were lower or similar. Mata-Torres et al. [17] carried out a simulation of a CSP + MED plant with fossil back-up considering a seawater pumping system to the plant's location. Results of this work showed the existence of optimum size of the MED plant that minimizes the Levelized Cost of Water (LCOW). Lastly, Valenzuela et al. [18]

* Corresponding author.
*E-mail addresses:* cnmata@uc.cl (C. Mata-Torres), azurita1@uc.cl (A. Zurita), jcardemil@ing.uchile.cl (J.M. Cardemil), rescobar@ing.puc.cl (R.A. Escobar).

https://doi.org/10.1016/j.enconman.2019.04.023
Received 7 January 2019; Received in revised form 19 March 2019; Accepted 6 April 2019
Available online 17 April 2019
0196-8904/ 

**Nomenclature**

| | |
|---|---|
| [A] | Incident matrix |
| $a_{ch}$ | Chemical exergy, kW |
| $A_f$ | Amortization factor, dimensionless, dimensionless |
| $b_i$ | Brine stream |
| $b_{mix1}$ | Mixed brine stream |
| $b_{mix2}$ | Brine output stream of the recovery system |
| $c_{ex}^*$ | Average unit exergy cost, dimensionless |
| $c_z^*$ | Average unit thermoeconomic cost, $/MWh or $/m3 |
| $cd_i$ | Condensate distillate stream |
| $c_{ex}$ | Unit exergy cost, dimensionless |
| $c_z$ | Unit thermoeconomic cost, $/MWh or $/m3 |
| $C_i$ | Exergy cost, kW |
| $\dot{C}_i$ | Thermoeconomic cost, kW |
| $dsh_i$ | Desuperheater distillate stream |
| $[Ex_i]$ | Exergetic cost vector |
| $f_i$ | Feed-water stream |
| $f_{O\&M}$ | Operation and maintenance factor, dimensionless |
| $f_{rh}$ | Ratio of the investment cost of the reheater from the investment cost of the boiler |
| g | Gravity constant, $m/s^2$ |
| h | Enthalpy, kJ/kg |
| i | Discount rate, dimensionless |
| $L_{pipe}$ | Length of the pipe, m |
| $\dot{m}$ | Mass flow rate, kg/s |
| n | Plant lifetime, y |
| $N_{effects}$ | Number of effects, dimensionless |
| $O_{time}$ | Annual operation time, h |
| P | Power, kW |
| Pr | Pressure, MPa |
| s | Entropy, kJ/(kg K) |
| $s_{cw}$ | Seawater cooling water stream |
| $s_{in\_1}$ | Seawater input stream of the pumping system |
| $s_{in\_2}$ | Seawater input stream of the MED condenser |
| $st_{in}$ | Steam input stream from the turbine exhaust |
| $st_{out}$ | Condensate output stream |
| T | Temperature, ˚C |
| TCI | Total Cost of Investment, $ |
| U | Overall heat transfer coefficient, kW/(K $m^2$) |
| UA | Heat exchanger thermal capacity, kW/K |
| V | Fluid velocity, m/s |
| $vd_i$ | Vapor distillate stream |
| w | Water or salt mass fraction of the seawater, dimensionless |
| $\dot{X}_{cv}$ | Exergy change within the control volume, kW |
| $\dot{X}_{dest}$ | Destroyed exergy rate, kW |
| $\dot{X}_i$ | Exergy rate, kW |
| $\dot{X}_{in}$ | Input exergy rate to the system, kW |
| $\dot{X}_{products}$ | Products exergy rate, kW |
| $\dot{X}_{waste}$ | Waste exergy rate, kW |
| $\dot{Z}$ | Purchase cost rate, $/h |

*Greek symbols*

| | |
|---|---|
| μ | Chemical potential, kJ/kg |
| $\eta$ | Efficiency, dimensionless |
| ψ | Physical exergy kJ/kg |

*Subscripts and superscripts*

| | |
|---|---|
| amb | Ambiental |
| boi | Boiler |
| ch | Chemical |
| cond | Condenser |
| dea | Deaerator |
| ex | Exergetic |
| gen | Generator |
| MED_i | MED effect electric consumption |
| MED_t | MED plant and P/R system required power |
| p_MED | Seawater pumping system power |
| tur_MED | Recovery system turbine power |
| o | Reference condition |
| ph | Physical |
| rh | Reheat |
| ttd | Terminal temperature difference |
| sg | Steam generator |
| st | Steam turbine |
| z | Thermoeconomic |
| II_law | Second law |
| * | Average |

*Abbreviations*

| | |
|---|---|
| ACC | Air Cooled Condenser |
| BPE | Boiling Point Evaporation |
| CFWH | Closed Feed-Water |
| CSP | Concentrating Solar Power |
| EES | Engineering Equation Solver |
| HTF | Heat Transfer Fluid |
| HX | Heat Exchanger |
| LCOE | Levelized Cost of Electricity |
| LCOW | Levelized Cost of Water |
| MED | Multi-Effect Distillation |
| MS | Molten Salts |
| MENA | Middle East and North Africa |
| NEA | Non-Equilibrium Allowance |
| P/R | Pumping and recovery |
| Pout 1 | First power output profile |
| Pout 2 | Second power output profile |
| RC | Rankine Cycle |
| RO | Reverse Osmosis |
| TTD | Terminal Temperature Difference |
| UAE | United Arab Emirates |

performed a study of a CSP + MED plant integrated with a photovoltaic (PV) plant, where the CSP system works as a back-up of the PV system, obtaining two different configurations that minimize the Levelized Cost of Electricity (LCOE) and LCOW and identifying a domain of solutions that allows minimizing both costs.

In these studies, it has been observed that during the assessment of a CSP + MED plant is common for CSP and MED plants costs to be allocated into LCOE and LCOW, separately; which means that the CSP cost only affects the LCOE, while the MED cost is allocated to the LCOW. The only exception is a fraction of the CSP plant cost that is allocated to the LCOW as a function of the electricity consumption of the MED plant and the seawater pumping system. In this way, the internal interactions between the systems are not accounted for the cost distribution (such as the use of the exhaust steam of the turbines to drive the MED plant). For instance, different methods have been studied in the literature to obtain the cost allocation in cogeneration plants. Wang and Lior [19] performed an evaluation of several methodologies to carry out a fuel allocation cost of a gas turbine plant coupled to a thermal vapor-compression MED (MED + TVC) plant. Results show that the exergy cost formation methodology, which is based on a comprehensive analysis of exergy destruction, allow computing the cost allocation with high detailed information. Leiva-Illanes et al. [20] presented a comparison between the levelized cost and the thermoeconomic methods to assess the product cost of a solar polygeneration

plant, obtaining that the thermoeconomic method constitutes a more rational cost allocation method, which is recommended for a precise analysis of a multi-purpose plant.

These studies indicate that the cost allocation method based on exergy flows and cost distribution (exergy cost and thermoeconomic analysis) are suggested to evaluate in detail the formation cost within a plant with different products. In this way, these methods have been implemented by [21–25] to assess the performance of solar power plants integrated with desalination technologies, determining the best design or operating conditions of the systems. Ortega-Delgado et al. [21] carried out a comparison between thermal desalination and RO technologies integrated to a CSP plant performing a sensitivity analysis varying the costs of the solar field, the MED, the RO, the discount rate and the capacity factor. With this methodology, they obtained that the RO scheme produces water at a lower cost than thermal desalination. Leiva-Illanes et al. [23] performed a thermoeconomic analysis of a solar polygeneration plant, obtaining that the criterion to optimize the plant design should be to minimize the total thermoeconomic cost, and the best configuration obtained considered the MED plant replacing the condenser.

Furthermore, the above approaches use the cost allocation analysis at low disaggregation level, which simplifies the number of streams evaluated. However, this approach does not represent the cost formation of each stream of the plant in detail. The use of medium or high disaggregation levels (i.e. performing the analysis for each component of the system) could give an in-depth analysis of the cost formation process of each stream that allows assessing a more accurate cost allocation. For example, Piacentino [26] performed a detailed thermoeconomic analysis of a MED + TVC plant, in which the seawater, freshwater, and brine exergy flows were split into their chemical and thermal fraction and the exergy efficiency was calculated at the subcomponent level to acquire an in-depth understanding of the whole formation process and the destroyed exergy distribution. Results indicated a water cost variation throughout the plant, where the contributions of the last effects were higher. Also, Catrini et al. [27] performed a thermoeconomic analysis for combined heat and power steam cycle integrated with a MED + TVC plant, obtaining that the water unit cost is significantly higher in comparison to the electricity cost, due to higher exergy destruction involved in the production process of the water. Moreover, it is performed a parametric analysis in function of the turbine extraction pressure and the number of MED units to understand their effect on both product costs. Leiva-Illanes et al. [28] carried out a exergy cost analysis of a solar polygeneration plant to analyze the exergy cost formation of the products and determine the key equipment which the design could be improved, resulting that the solar collectors, the evaporator and the productive sub-systems (MED, refrigeration and process heat plant) are the key components that contribute to the products formation cost.

In summary, the cost allocation method considers the cost and the processes involved in the production of each stream of the plant, but a detailed analysis requires to perform the analysis at the component level. In that context, to the best of authors' knowledge, there is no study in the literature performing a detailed exergy cost and thermoeconomic analysis of a CSP + MED plant, considering a high disaggregation level. Moreover, the thermoeconomic analyses of cogeneration plants have been performed at nominal conditions, but, considering that a CSP + MED plant operates using solar radiation as the main energy source, its operating conditions are highly variable due to the nature of the availability of solar radiation. These variations enforce the power cycle of the CSP plant and the MED plant to operate at part-load conditions during several periods of the day, which induces additional complexity to the exergy analysis and the fuel cost allocation. Besides, the ambient temperature also varies during the day, changing the exergy and cost allocation of the waste stream.

In this study, it is presented a detailed exergy cost formation and thermoeconomic analyses applied to a Rankine Cycle (RC) fed by solar molten salts (MS), and coupled to a MED plant (RC + MED). The aim is to assess the distribution of exergy destructions, exergetic cost formation and the thermoeconomic cost of the final products. The study considers transient conditions such as the variation of the ambient temperature and the plant part-load operation due to variations on the MS mass flow rate. Moreover, a sensitivity analysis varying the MED plant capacity and the location of the plant respect to the sea level, as well as, the analysis of an operational day of the RC + MED plant considering two power output profiles were carried out. The analyses presented herein take into account parasitic exergy losses that have not been commonly considered in the literature, for instance: the exergy and cost expenses by the pumping system from the sea to the MED plant location, and the electricity consumed by the MED plant and the RC condenser. Additionally, the model includes the possibility of using the exergy associated to the energy potential of the brine to produce useful work. Therefore, the detailed model developed allows to accurately assess the actual exergy and thermoeconomic cost of the final products of the RC + MED plant, under the different conditions and configurations.

## 2. System description

The RC + MED plant analyzed herein consist of a steam RC coupled with a MED plant in parallel with the condenser of the power cycle. The RC is fed by solar molten salts since it constitutes the typical heat transfer fluid (HTF) employed in Central Receiver CSP plants. The MED plant uses a fraction of the exhaust turbine steam to provide heat to the desalination process, and the condenser dissipates the heat of the remaining flow. Also, a seawater pumping system from the sea to the RC + MED plant location, and an energy recovery system of the resultant brine that is returned to the sea (P/R System) were considered in the model. The electric consumption of the MED plant, the seawater pumping system and the condenser were included. In Fig. 1 is presented a detailed scheme of the RC + MED plant. Moreover, in Fig. 2 shows where is located the RC + MED plant respect to the sea, considering that the P/R system is located at the coast, and the seawater and the resultant brine are transported into the pumping and discharge pipes.

### 2.1. Rankine cycle

The Rankine Cycle consists of a 100 MW plant powered by a molten salt (MS) mixture (60% $NaNO_3$ and 40% $KNO_3$) as HTF. This RC is the typical power cycle that is coupled to a CSP plant, which design temperature of the MS is usually set to 565 °C. Specifically, the RC modeled herein considers re-heating, a throttling valve to control the part-load operation, three regeneration heat feeders (two closed feed-water heaters –CFWH– and an open feed-water heater or deaerator), and an Air-Cooled Condenser (ACC). For the design conditions of the stand-alone RC, the condensing pressure is defined as the saturation pressure at 25 °C higher than the ambient temperature [29]. However, when considering the MED plant coupling in parallel to the ACC, the condensing pressure of the RC + MED plant is assumed as 31.2 kPa, in order to ensure a saturation temperature of 70 °C. That temperature is required to enable the MED plant [17]. Moreover, for the design conditions, it is considered a pinch point difference of 15 °C and 20 °C in the steam output of the superheater and the reheater respectively, and 30 °C in the water stream input of the evaporator. The CFWH considered a design terminal temperature difference (TTD) of 5 °C, and the deaerator a fixed pressure of 170 kPa. Lastly, the input condensate stream of both RC pumps is defined as to have a 1 °C of subcooling.

The RC model considers part-load operation using the constant pressure control, that keeps the same working pressure in the boiler and the part-load operation by using throttle valves. The part-load operation is limited to 30% of the design MS mass flow rate, which was considered to lower operation point that the steam turbines can work. The evaporators, super-heater, re-heater, and CFWH consider a design

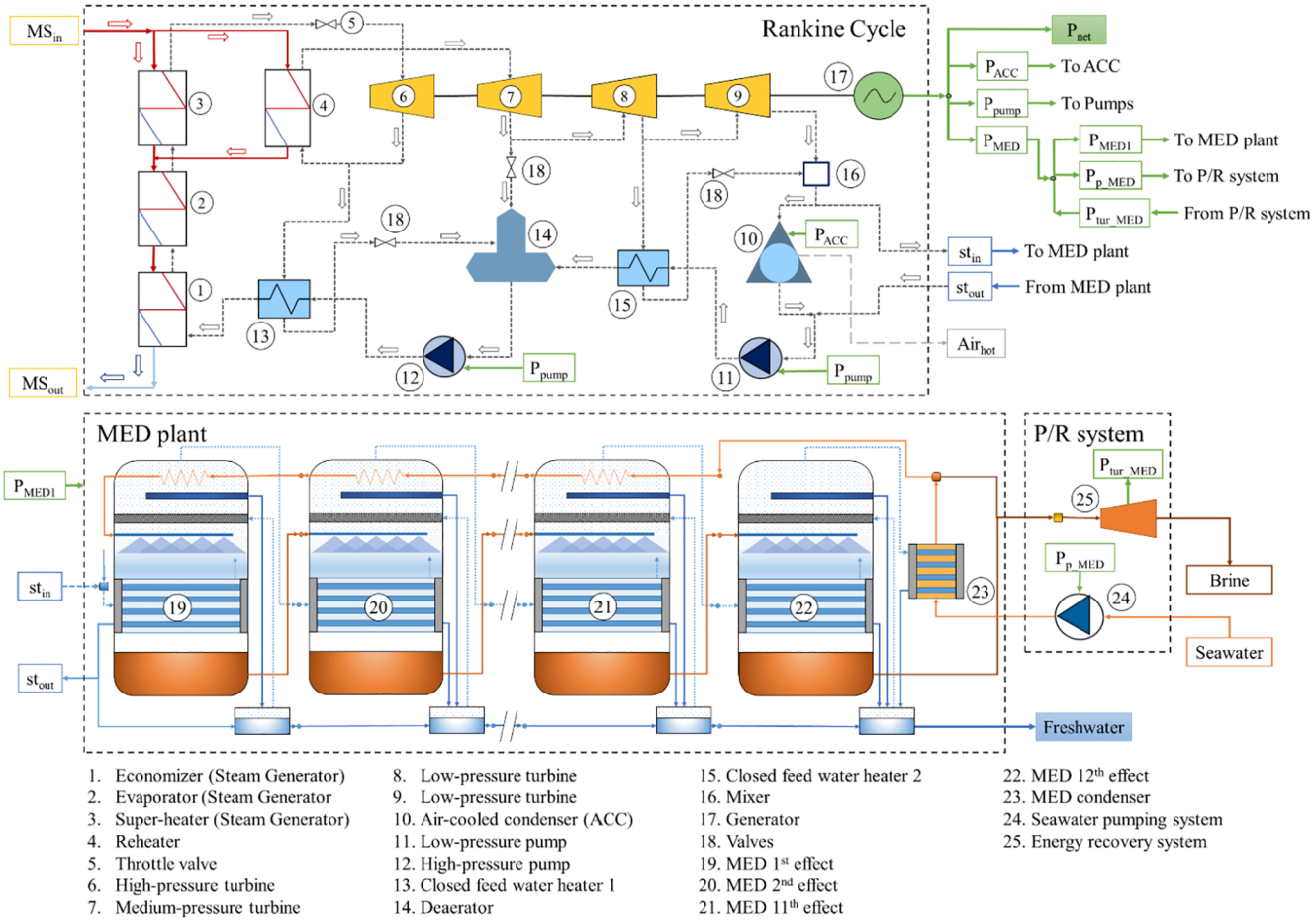


**Fig. 1.** The RC + MED detail plant scheme.

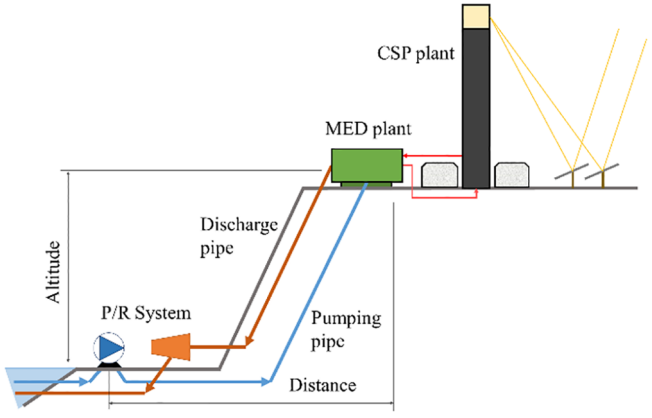


**Fig. 2.** The RC + MED plant location respect to the sea.

exchanger transfer conductance-area product (UA), while the effective UA is calculated by the correlation presented by Patnode [29]. Turbines' part-load operation was modeled with the Stodola's cone law, and the isentropic efficiency of the turbine variation was calculated according to the correlation proposed by Patnode [29]. Finally, at part-load operation, the MED plant is firstly powered, and the ACC is activated only when a remaining steam flow exists.

### 2.2. MED plant

The MED plant model consists of a forward-feed plant of 12 effects and 11 pre-heaters. This plant incorporates a condenser in the final effect to condensate the vapor distillate produced and heating the input seawater. The developed model is based on the models described by Palenzuela et al. [30] and Ortega-Delgado et al. [31,32]. These models describe in detail the thermodynamic performance of a MED plant, considering the flash evaporation of the brine in each effect, and the flash evaporation of the distillate in the flash boxes. Also, the thermal losses as the Boiling Point Elevation (BPE) and the Non-Equilibrium Allowance (NEA) were calculated following the equation presented in [33,34], and pressure losses were considered decreasing 0.2 °C the temperature of the vapor distillate between the effects. The model considers that the freshwater produced is free of salt, and the resultant brine of the last effect has a maximum salinity of 72 $g_{salt}/kg_{water}$. Moreover, the model incorporates the assessment of the operation of the MED at part-load or non-design conditions. For this, firstly, the effects, preheaters, and condenser heat exchanger areas were calculated for the design conditions, and then, there are fixed for the calculation of the plant operation. The overall heat transfer coefficients (U) were calculated using the correlation proposed by El-Dessouky and Ettouney [33]. In addition, a de-superheater was considered before the first effect, aiming to reduce the temperature of the steam inlet to the saturation temperature. That de-superheater considers the utilization of the freshwater obtained in the last effect of the MED plant, to remove the heat. Finally, the influence of the non-condensable gases was not considered in this model, since its effect is insignificant.

### 2.3. Seawater pumping and brine energy recovery system

The seawater pumping system model considers a simple piping scheme and a pump, in which the seawater is pumped to the RC + MED plant location. The model calculates the piping losses and the hydraulic

power required by the pump by the Darcy-Weisbach equations and the energy balance. Then, the electric power requirement is calculated considering a fixed pump efficiency. On the other hand, the brine energy recovery system rescues the potential energy of the resultant waste at the MED plant. Indeed, the MED plant has two main waste streams: the brine of the last effect and the excess seawater that is used in the MED plant condenser (cooling seawater). These streams are mixed and returned to the sea through this system. The energy recovery device consists of a hydraulic turbine which produces work to reduce the total electric requirement from the pumping system. As well as the pumping system, the piping losses are calculated and the hydraulic head at the final of the pipeline is determined. Then, the work is calculated considering the turbine efficiency.

## 3. Methodology

The RC + MED plant analysis was performed by coupling two computational tools: Engineering Equation Solver (EES) software to assess the thermodynamic and exergy performance of the RC, the MED plant and the pumping and recovery system (P/R system); and MATLAB R2016b to carry out the exergetic cost and thermoeconomic analyses. This section describes the analysis performed and the computational process.

### 3.1. Energy analysis

The RC + MED plant performance was analyzed using EES in two different decks. The RC model assesses the thermodynamic states of all the streams and the components in the RC, considering mass and energy balance equations in steady-state conditions, as well as heat transfer equations for the heat exchangers. The model first calculates the thermodynamic performance at design conditions, determining the design UA. Then, the thermodynamic performance at operating conditions is estimated considering the temperature and mass flow rate of the MS, and the ambient temperature as inputs. All model's calculations are carried out considering steady-state conditions.

The MED plant model describes the thermodynamic performance of all the streams for each effect of the MED plant and the performance of the P/R system. The disaggregation level of the MED model considers for each effect: the main heat exchanger, the feed water preheater, the distillate flash box, and the condensate water mixer. The mass and energy balance and the heat transfer equations are applied for each one of these subcomponents of the effect. Further information about the mathematical model can be found in Ortega-Delgado et al. [32], which shows the equations considered in detail for each one of subcomponents. Moreover, the MED plant electric consumption is calculated in terms of the freshwater production, considering a value of $1.5\,kWh_e/m^3$ [35], which takes into account the use of water and vacuum pumps. Regarding the P/R system, the head losses are calculated using the Darcy-Weisbach equation. The friction factor is calculated in terms of the length, diameter and relative roughness of the pipe, and the kinematic viscosity of the fluid. Then, the total head at the pump and at the recovery system are calculated by applying energy balance. The electric consumption of the pump and the turbine work are calculated computing their respective efficiencies. It is worth to mention that other piping losses are not considered. In the first instance, the MED model is used to calculate design parameters in terms of the MED plant capacity, the location's altitude and the distance from the sea. At this point, the heat exchange areas of each effect, preheaters and the condenser are calculated. Then, the performance of the MED plant is obtained, considering the steam mass flow rate and the enthalpy of the turbine exhaust steam, the ambient temperature, the seawater mass flow rate and its salinity as inputs.

Table 1 presents the design parameters considered in the modeling of the RC, MED and P/R systems. These parameters include the nominal temperature and mass flow rate of the MS, the ambient temperature, the salinity and temperature of the input seawater.

### 3.2. Exergy analysis

A preliminary exergy analysis was carried out to calculate the exergy flow of all the streams considered in the RC + MED plant. The exergy is a property which defines the maximum useful work that could be obtained from a system or stream at a specified state in comparison to a reference state. In an exergy analysis, it is useful to decompose the exergy flow into their physical and chemical exergy. The physical exergy represents the maximum amount of work that can be obtained from a system as its pressure and temperature are changed to the reference state. In contrast, the chemical exergy is related to the difference in the chemical potential of the substance that changes its chemical composition or concentration compared to the reference state [36,37]. The exergy analysis in this work was carried out in EES, using the software library and literature reference for specific streams.

In this analysis, the physical exergy was calculated for all the RC streams (molten salts and water steam) and the MED plant streams (seawater, water, and brine). The physical exergy is denoted by $\psi$, and it is defined as:

$$\psi = (h - h_o) - T_o(s - s_o) + gz + \frac{V^2}{2} \tag{1}$$

where $h$ and $s$ are the enthalpy and entropy of the stream at a given state, respectively; while $h_o$, $s_o$ and $T_o$ are the properties at the reference state. The other two terms are the potential and kinetic energy that consider the gravity constant ($g$), altitude ($z$) and the fluid velocity ($V$). For this analysis, the kinetic energy was not considered, and the potential energy was only considered for the MED plant streams, associated to the seawater, the freshwater and the brine, because they are the only streams that present a significant altitude variation. Moreover, the enthalpy and entropy of the seawater, freshwater and brine were calculated using the correlation proposed by Sharqawy et al. [38]. Then, the physical exergy rate ($\dot{X}_{ph}$) is given by [37]:

$$\dot{X}_{ph} = \dot{m}\psi \tag{2}$$

where $\dot{m}$ is the mass flow rate of the stream. In the analysis of the MED plant, it is required to calculate the chemical exergy of the streams related to the seawater, the freshwater or the brine. This exergy was considered separately from the physical exergy. For the reference state, it was established a salinity of $32\,g_{salt}/kg_{water}$ and a seawater

**Table 1**
Design parameters of the RC, MED plant and P/R system.

| | Unit | Value |
|---|---|---|
| Nominal MS mass flow rate | kg/s | 650 |
| Nominal MS input temperature | °C | 565 |
| Nominal MS output temperature | °C | 295 |
| Evaporator UA | kW/K | 2098.55 |
| Super-heater UA | kW/K | 1439.28 |
| Re-heater UA | kW/K | 720.38 |
| CFWH 1 UA | kW/K | 1359.50 |
| CFWH 2 UA | kW/K | 484.74 |
| Superheated steam pressure | kPa | 10,000 |
| Steam extraction pressure 1 (CFWH 1) | kPa | 2200 |
| Steam extraction pressure 2 (Deaerator) | kPa | 600 |
| Steam extraction pressure 3 (CFWH 2) | kPa | 70 |
| High-pressure turbine efficiency | – | 0.90 |
| Low-pressure turbine efficiency | – | 0.86 |
| Pump efficiency | – | 0.85 |
| Input seawater temperature | °C | 20 |
| Cooling seawater stream temperature | °C | 35 |
| Brine temperature at last effect | °C | 40 |
| Seawater salinity | g/kg | 32 |
| Brine exhaust salinity | g/kg | 72 |
| Gain Output Ratio (Nominal conditions) | – | 9.64 |
| Pump and turbine efficiency (P/R system) | – | 0.8 |

temperature of 20 °C. The chemical exergy of a flow stream is denoted by $a_{ch}$, and it is determined by [38,39]:

$$a_{ch} = \sum_{i=1}^{n} w_i(\mu_i^* - \mu_i^0) \tag{3}$$

where $w_i$ is the water or salt mass fraction (dimensionless) of the seawater, the brine or the water, which is in terms of the salinity of the stream, and $\mu_i$ is the chemical potential of the water or the salts in seawater in kJ/kg that are determined by differentiating the total Gibbs energy function with respect to the composition [38]. The chemical potential is calculated by different correlations proposed by Sharqawy et al. [39]. The $\mu_i^*$ is calculated with the stream salinity and the reference temperature, while the $\mu_i^0$ is calculated with the seawater reference salinity and temperature. It is worth to mention that for the present analysis; the chemical exergy is only expressed in terms of the salinity of the stream. So, given the salinity reference, the freshwater chemical exergy (considered free of salt) can be defined as 2.35 kJ/kg. Then, the chemical exergy rate ($\dot{X}_a$) is given by:

$$\dot{X}_a = \dot{m} a_{ch} \tag{4}$$

When an exergy balance of a system, component or subcomponent is performed, it can be identified the lost work potential caused by the irreversibilities or exergy destructions. The irreversibilities can be explained by friction, chemical reactions, heat transfer, among other processes, which always generate entropy and destroy exergy. Thus, the exergy balance of a control volume is expressed as [37]:

$$\sum_{in} \dot{X}_{ph} - \sum_{out} \dot{X}_{ph} + \sum_{in} \dot{X}_a - \sum_{out} \dot{X}_a - \dot{X}_{dest} = \frac{d\dot{X}_{CV}}{dt} \tag{5}$$

where $\dot{X}_{dest}$ is the destroyed exergy rate, and $\dot{X}_{CV}$ is the exergy change within the control volume. When steady-state is considered, the exergy change rate is neglected. In this way, the exergy destruction can be calculated for each component of the RC + MED plant. For the present analysis, the exergy balance was applied to all the components of the RC + MED (47 components), with each effect of the MED plant was considered as a component. Additionally, the net electricity and the freshwater chemical exergy were considered as products of the plant. Indeed, the freshwater physical exergy was considered a waste of the MED plant, since to the main purpose of the plant is to produce a quantity of freshwater, which is related to the amount of chemical exergy obtained.

Finally, two definitions for the exergy efficiency were considered to evaluate the efficiency of the plant. The first one is commonly known as the second law efficiency ($\eta_{II\_law}$), which measure how efficient is the plant compared to an ideal plant, considering the input exergy to the system ($\dot{X}_{in}$) and the total exergy destruction throughout the plant, and the latter is commonly denominated exergetic efficiency ($\eta_{ex}$), which compares the exergy of the products with the exergy input [37].

$$\eta_{II\_law} = 1 - \frac{\sum \dot{X}_{dest}}{\sum \dot{X}_{in}} \tag{6}$$

$$\eta_{ex} = 1 - \frac{\sum \dot{X}_{dest} + \sum \dot{X}_{waste}}{\sum \dot{X}_{in}} = \frac{\sum \dot{X}_{products}}{\sum \dot{X}_{in}} \tag{7}$$

### 3.3. Exergetic cost analysis

The exergetic cost analysis allows assessing the process of cost formation of the products from an exergy point of view. This analysis permits to identify how the exergy destructions and the exergy of waste flows are allocated to the final products. Through this analysis is possible to determine the amount of resources required to generate a specific product. The analysis was performed by MATLAB, using the numeric values of physical and chemical exergies obtained from the procedure implemented in EES. The analysis consists of a linear equation system given by,

$$[A] \times [C_i] = [Ex_i] \tag{8}$$

where the matrix [A], known as the incident matrix, summarizes the flow connections between each component of the plant, and the exergy cost ($C_i$) considers the consumption of exergy to produce a given flow and depends on the conditions and the processes employed to produce it. Hence, the exergy cost vector ($[C_i]$) is the one to be evaluated, and the exergetic cost vector ($[Ex_i]$) is the solution, that only takes the fuel exergy values for the respective auxiliary equation [23,40]. This system can be solved by using matrix algebra [36,37,41]. The equation system is represented by the exergy cost ($C_i$) balance equation for each component as:

$$\sum C_{in} - \sum C_{out} = 0 \tag{9}$$

where the inputs are the resources from other components or the environment (known as fuel), and the outputs are the products that could be considered as resources for other components or for the environment (known as final products). For each component, according to its own process, the fuel is partially transformed into products and destroyed by the irreversibilities, therefore, the cost of the irreversibilities is allocated to the products. Consequently, the exergy cost of a given stream is related to the exergy rate ($\dot{X}_i$) through the unit exergy cost ($c_{ex\_i}$) by:

$$C_i = c_{ex\_i}\dot{X}_i \tag{10}$$

There are more than one input and output for some components, which implies that there would be more streams than components. In such cases, it is required to use auxiliary equations. These equations correlate or match the unit exergy cost of different streams to complete the equation system. Furthermore, the matrix is determined by the exergy analysis, which depends exclusively on the physical scheme of the plant and the thermodynamic analysis. In this study, the RC + MED plant presents 148 streams and 47 components. Thus, several auxiliary equations were considered. These equations were separated into three main groups: RC equations, MED plant equations, and P/R system equations. More details about the auxiliary equations are described in Appendix A.1. Finally, the exergetic cost vector only considers the fuel exergy of the hot MS mass flow rate and the physical exergy of the seawater from the sea.

### 3.4. Thermoeconomic analysis

The thermoeconomic analysis combines the thermodynamics evaluation based on the exergy analysis and the economic analysis providing useful information of the cost-effective design or operation of a system that could not be achieved by conventional energy and economic analyses. The aim is to assess the monetary value of each stream of the system. Thus, the thermoeconomic cost represents the monetary value of the resources allocated in a specific stream. This methodology allows allocating the economic cost of plant components to the products based on the exergy analysis, the exergy destruction and the waste exergies. The analysis consists of a linear equation system similar to the one presented in Section 3.3:

$$[\dot{A}] \times [\dot{C}_i] = [\dot{Z}_i] \tag{11}$$

where the matrix $[\dot{A}]$ summarize the thermoeconomic cost balance and has the same structure than the incidence matrix described in the previous section, which only depends on the physical system scheme. The cost vector ($[\dot{C}_i]$) is the one to be determined and the thermoeconomic vector ($[\dot{Z}_i]$) includes the $\dot{Z}_i$ factor per component and the unit thermoeconomic cost of the fuels, which is determined by an economic analysis. Hence, the equation system is composed by the thermoeconomic cost ($\dot{C}_i$) balance equation for each component given by:

$$\sum \dot{C}_{in} - \sum \dot{C}_{out} + \dot{Z}_i = 0 \tag{12}$$

where the purchase cost rate of the component ($\dot{Z}_i$) is included. Thus, the thermoeconomic cost rate ($\dot{C}_i$) considers the cost formation process to produce a given flow, which depends on the exergy performance and the cost of the components employed. Lastly, the cost rate is related with the exergy rate through the unit thermoeconomic cost ($c_{z\_i}$), and is defined as follows [36,37]:

$$\dot{C}_i = c_{z\_i}\dot{X}_i \tag{13}$$

Furthermore, the auxiliary equations were the same applied for the exergetic cost analysis, changing only two of them: the unit thermoeconomic cost of the seawater is null, and the unit thermoeconomic cost of the hot MS was fixed.

The thermoeconomic vector was calculated performing an economic analysis, where the total cost of investment (*TCI*) for each of the components was computed considering cost correlations available in the literature [26,42–44]. The cost function details are described in Appendix A.2. Then, the purchase cost rate of each component is obtained by the following expression in $/h:

$$\dot{Z}_i = \frac{A_f + f_{O\&M}}{O_{time,i}} TCI_i \tag{14}$$

where the $f_{O\&M}$ is the operation and maintenance factor that was set to 5%, $O_{time,i}$ is the annual operating time of the component in hours and the $A_f$ is the amortization factor of the investment cost expressed as,

$$A_f = \frac{i(1+i)^n}{(1+i)^n - 1} \tag{15}$$

where $i$ is the discount rate, and $n$ is the plant technical lifetime. The selected values were 5% and 30 years [45]. For this analysis, it was considered that all RC, MED plant and P/R system components have an availability of 80% during the year, while the ACC has an availability of 70%.

Regarding the MS unit cost, which is assumed as the fuel for the RC + MED plant, it was considered that are delivered by a CSP plant. Furthermore, it was considered an installation cost of 5$/W for the CSP plant and the TCI of 500 MM$. These values are a conservative cost of a CSP plant considering the recent literature [46]. Thus, the purchase cost rate was obtained, and the unit thermoeconomic cost of the MS stream was calculated considering the net exergy input (the difference between the exergy input of the hot MS stream and the exergy output of the cold MS stream) at nominal conditions. The MS unit thermoeconomic cost obtained was 42.87$/MWh, and it was remained fixed for the parametric analysis. Finally, as mentioned before, the final products of this analysis are the net electricity of the plant and freshwater chemical exergy. The units of these unit thermoeconomic cost were reported in $/MWh and $/m$^3$.

### 3.5. Computational procedure

A computational procedure was carried out, which consist of 5 sections that allow determining the plant's exergy balance and the thermoeconomic costs. Fig. 3 presents a flow diagram of this process, where each section is:

1. MED plant design using EES: the design configuration of the MED plant and the P/R system (HX areas of the effects, preheaters and the final condenser, diameter of the pipeline, design capacity of the pumping and recovery system) was calculated. Outputs of this section are the HX areas of the MED plant and the maximum design flow that the MED plant can take from the turbine exhaust stream.
2. RC model operation using EES: the design and operation of the RC were modeled. The exergy for each stream was evaluated according to the thermodynamic and the exergy performance. The output of this section is the steam mass flow rate, the enthalpy of the stream that feeds the MED plant, and the exergy vector of the RC cycle.
3. MED plant operation using EES: the operation of the MED plant and P/R system was calculated obtaining all the stream exergies for both systems.
4. Economic analysis: the cost rates of the different components are calculated considering several cost functions.
5. Exergetic cost and thermoeconomic analysis using MATLAB: the exergetic cost and the thermoeconomic analysis is carried out to finally determine the exergy, unit exergy and thermoeconomic costs.

## 4. Results and discussion

The analysis of the RC + MED plant was carried out varying the MS mass flow rate (part-load operation) and the ambient temperature to assess the exergy destruction distribution, the exergetic cost formation and the thermoeconomic cost of the final products. Also, the MED plant size and the plant's altitude and distance from the sea location was evaluated. The design conditions were defined as: a MS mass flow rate of 650 kg/s (which represent the full-load operation of the plant), a MS hot temperature of 565 °C, an ambient temperature of 25 °C, a MED plant size of 40,000 m$^3$/day, a location's altitude of 100 m and a distance from the sea of 20 km. The parametric analyses were performed varying one design conditions, keeping the other constant.

### 4.1. Exergy performance results

The exergy analysis was performed under design conditions, which are summarized in Table 2, showing the inputs and outputs considered in the exergy analysis for a standalone RC and a RC + MED fed by MS.

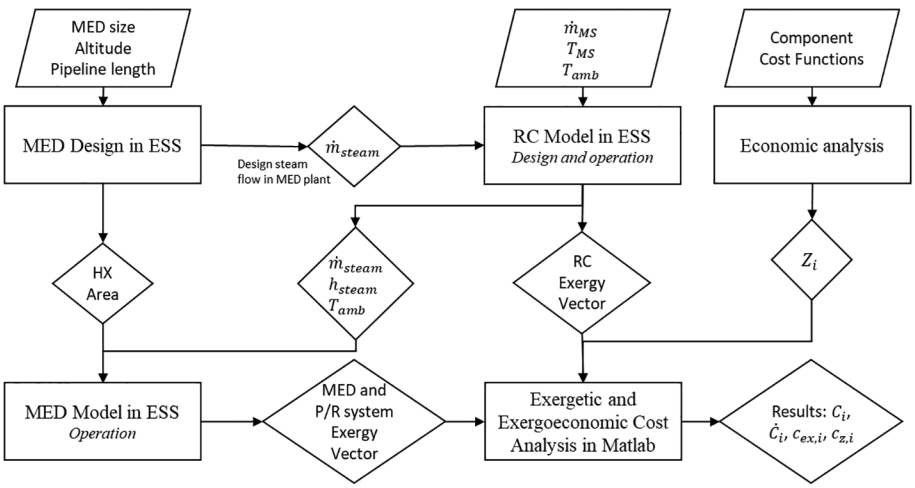


**Fig. 3.** Flow diagram of the computational process.

**Table 2**
Comparison between an RC and an RC + MED fed by molten salts.

| | Unit | RC | RC + MED |
|---|---|---|---|
| Nominal MS mass flow rate | kg/s | 650 | 650 |
| MS exergy input | MW | 155.13 | 155.13 |
| Seawater exergy input | MW | – | 0.33 |
| Net electricity | MW | 100.00 | 86.44 |
| Water (chemical exergy) | MW | – | 1.08 |
| Destroyed exergy | MW | 52.03 | 64.78 |
| Wasted exergy | MW | 2.41 | 3.17 |
| $\eta_{II\_law}$ | % | 66.46% | 59.94% |
| $\eta_{ex}$ | % | 64.90% | 56.30% |

Results indicate that the RC + MED plant produces 13.56 MW less of electricity than the standalone RC, due to the increase of the turbine exhaust pressure, the electric consumption of the MED plant and the seawater pumping system. In fact, 33% of this reduction is caused by the MED plant and seawater pumping total consumption, and the other 67% is a result of increasing the turbine's exhaust pressure. On the other hand, the chemical exergy of the freshwater has a very low value compared to the other product flow, considering that it is used a significant amount of exergy to be produced. The operation of the MED plant presents a high exergy destruction rate, and the waste streams exergy are higher than the final product: the freshwater chemical exergy. However, this chemical exergy is equivalent to 1654.9 $m^3$/h freshwater production, which is a relevant production to be considered, thus, the freshwater production is associated with a high-exergy destruction process. In this way, coupling the MED plant implies an increase on the turbine's exhaust stream exergy, which results in higher exergy destruction in the dissipative components after the turbine (the MED plant and the ACC). In terms of efficiency, the RC + MED is not more efficient than a standalone RC since the $\eta_{II\_law}$ and $\eta_{ex}$ of the RC + MED are 9.8% and 13.3% lower than the values obtained with the standalone RC, respectively. These findings are in agreement with results reported by Leiva-Illanes et al. [20], and Mata-Torres et al. [47] (previous study by the authors), in which the coupling of the MED plant decreases the exergy efficiency.

Fig. 4 shows the exergy destruction distribution on the main components of the RC + MED plant and the wasted exergy distribution. The main exergy destruction occurs in the steam generator where the high-temperature steam is produced. However, the dissipative components combined (the MED plant and the ACC) presents the second highest exergy destruction contribution, reaching 31% of the total. Thus, the condensing pressure of the dissipative components is the main factor that affects their exergy destruction, besides the fact that the MED plant allows recovering a small part as freshwater chemical exergy. The P/R system has a small contribution to the total exergy destruction; however, its influence can be more relevant varying the location of the plant with respect to the coast. On the other hand, the MED plant waste streams accounted for 76.6% of the total wasted exergy, half of that comes from the brine thermal and chemical exergy, whereas the other half comes from the freshwater thermal and potential exergy. Indeed, freshwater and brine output streams are obtained approximately at 40 °C, which is not useful for other production processes.

The exergy performance of the plant was evaluated considering a parametric analysis under part-load operation (varying the MS mass flow rate from 195 to 650 kg/s, which represents 30% to 100% of the capacity) and varying the ambient temperature (from 0 to 40 °C). Fig. 5 shows the total exergy destruction, the destroyed exergy distribution and efficiencies for both parametric analyses.

Under part-load operation (Fig. 5.a), exergy efficiencies ($\eta_{II\_law}$ and $\eta_{ex}$) decrease not linearly as the MS mass flow rate is reduced, achieving values 15% and 20% lower than at full-load operation, respectively. This evidences that fewer exergy outputs are produced at part-load operation, and the off-design operation of the RC + MED plant increases the destroyed exergy rate, even when the total exergy destruction tends to decrease. Also, the contribution of each component to the total destroyed exergy changes as the MS mass flow rate is lower. The main change occurs on the throttle valve, which its contribution raises to 15% at the lowest MS mass flow rate. This is caused by the input pressure reduction at the high-pressure turbine that is calculated using the Stodola's relation. On the other hand, the contribution of the MED plant and the P/R system increases until the RC operates at 70% of its capacity. At this point, the ACC is activated. Therefore, under a part-load operation between 70 and 100%, the ACC destroyed exergy increases while the MED plant and the P/R system destroyed exergy remains stable.

When the ambient temperature varies (Fig. 5.b), $\eta_{II\_law}$ decreases at higher temperatures, while the $\eta_{ex}$ increases. This difference on the behavior presented by the efficiencies is produced as the $\eta_{II\_law}$ only considers the total exergy destruction of plant, while the $\eta_{ex}$ also considers the wasted exergy, which decreases for higher temperatures due to the ambient temperature is closer to the temperature of waste streams. Thus, for lower ambient temperatures, the exergy waste increases considerably resulting in a decrease of the $\eta_{ex}$. Moreover, the $\eta_{II\_law}$ varies between 62% and 58%, while the $\eta_{ex}$ varies from 52% to 57%. Also, the destroyed exergy slightly increases with the rise of the ambient temperature, but, the exergy destruction contribution remains almost stable for all components. The most relevant differences are observed in the ACC and MED plant's contributions, increasing the ACC contribution as the ambient temperature is lower, while the MED plant contribution decreases. This happens because the heat transfer in the ACC, between the steam and the air, is produced with a larger

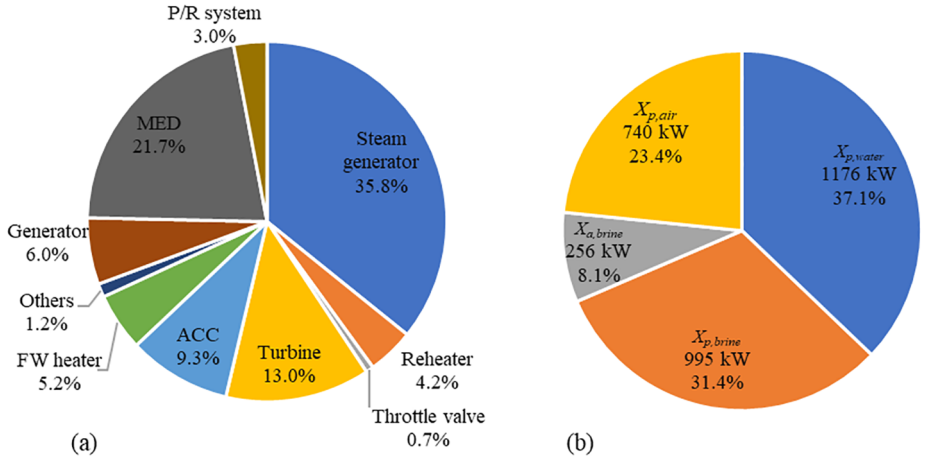


**Fig. 4.** (a) Distribution of the destroyed exergy per component, and (b) Distribution of the wasted exergy for the RC + MED plant.

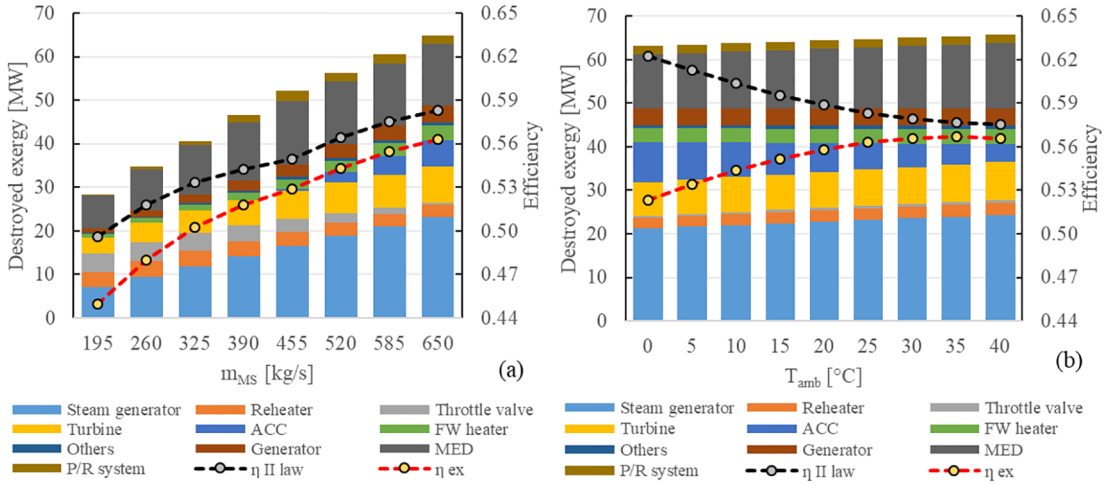


**Fig. 5.** Destroyed exergy and efficiency for:(a) part-load operation and (b) ambient temperature variation.

temperature difference at lower ambient temperatures increasing the entropy of the process. Finally, the steam generator and the turbines have a slight increase in the destroyed exergy contribution for higher temperatures. In a previous study by the authors [47], it were found the same tendency in the exergy efficiency and destroyed exergy distribution of the plant, so it is evidenced that steam generators and dissipative components are the more relevant to evaluate its design and operation. Furthermore, the results presented by Kouta et al. [22] and Elsafi [48] agree with these findings related to the relevance of the dissipative components. It is important to notice that the thermodynamic performance and the exergy products of the RC + MED plant is constant for all the temperatures (only changing the air mass flow rate at ACC), yet, the physical exergies change with the temperature variation.

### 4.2. Exergetic cost analysis

The exergetic cost analysis was performed considering a parametric variation on the MS mass flow rate and the ambient temperature of the RC + MED plant. The products considered in the analysis were the net electricity and the freshwater chemical exergy. Also, as a point of reference, the exergy cost analysis of a standalone RC was taken into account, considering the net electricity as the only product. The exergy cost and unit exergy cost for both parametric analyses are presented in Fig. 6.

Fig. 6.a shows that the electricity exergy cost ($C_{el}$) linearly increases as the MS mass flow rate rises, while the water exergy cost ($C_w$) increases until the MS mass flow rate rises to 455 kg/s and then it remains

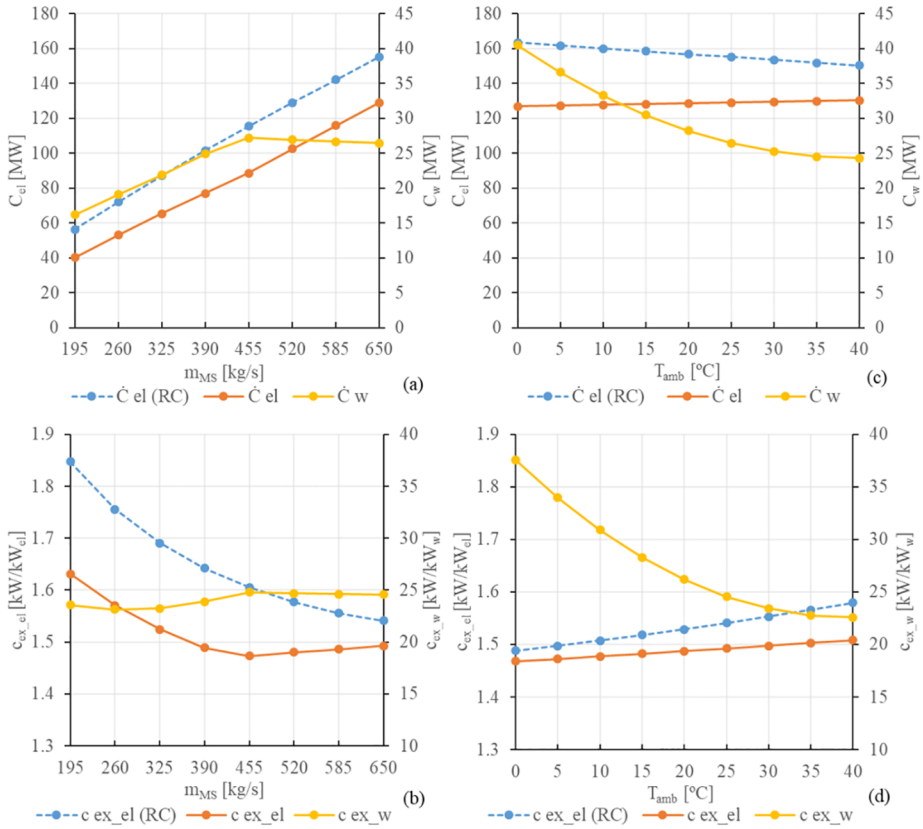


**Fig. 6.** Exergy cost and unit exergy cost of the electricity and water for (a-b) part load operation and (c-d) ambient temperature variation.

stable. In contrast, the unit exergy cost results show that the electric unit exergy cost ($c_{ex\_el}$) gradually decreases with the rise of the MS mass flow rate, but from 455 kg/s, remains almost stable (Fig. 6.b). The water unit exergy cost ($c_{ex\_w}$) presents a similar behavior, however, from 195 kg/s to 455 kg/s it has a smaller variation than the $c_{ex\_el}$ decreasing its value. Moreover, the largest variation exhibited by the $c_{ex\_el}$ in comparison to the full-load operation is about 9%, while for the $c_{ex\_w}$ is only 5%. These results expose that the destroyed exergy from the throttle valve under part-load operation is allocated in the $c_{ex\_el}$, while the $c_{ex\_w}$ has a lower destroyed exergy allocation decreasing its unit cost formation. Thus, the part load operation has a more significant influence on $c_{ex\_el}$ than $c_{ex\_w}$. Moreover, in Mata-Torres et al. [47], it was obtained that the exergy cost fraction of the water increases with a lower MS mass flow rate. This tendency is observed in Fig. 6.a, where the variation of the $C_{el}$ is sharper (ranging from more than 80 MW) than the $C_w$, which varies only 10 MW.

Regarding the ambient temperature variations, the exergetic cost analysis (Fig. 6.c) shows that the $C_{el}$ presents a similar numeric value for all temperatures, while the $C_w$ presents a non-linear variation, achieving higher values as the temperature is reduced. The unit exergy cost analysis (Fig. 6.d) shows that the $c_{ex\_el}$ slightly increases at higher temperatures, while the $c_{ex\_w}$ increases with a non-linear trend for lower temperatures. In this case, the largest variation of $c_{ex\_el}$ in comparison to the design conditions is about 3%, while for the $c_{ex\_w}$ is 67%. This high variation of the $c_{ex\_w}$ is attributed to the rise of the exergy waste at lower temperatures, which exergy costs are allocated to the water, and the $c_{ex\_el}$ slightly variation is for the increase of steam generator and turbines destroyed exergy contribution. These results indicate that the $c_{ex\_w}$ is highly dependent on the ambient temperature. Furthermore, the results are reinforced by the findings reported in [47], where the exergy cost fraction of the water decreases for higher temperatures, meaning the most of the exergy costs are allocated to the electricity for higher temperatures, decreasing both $C_w$ and $c_{ex\_w}$. However, the variation in the $C_{el}$ is small, so the variation is of the $c_{ex\_el}$ almost insignificant. Moreover, the $C_{el}$ and the $c_{ex\_el}$ from the RC + MED were lower than both exergy cost and unit exergy cost of electricity of the stand-alone RC, which evidences that the water production allocates a significant part of the destroyed exergy and the wasted exergy cost, decreasing the electricity cost allocation.

### 4.3. Thermoeconomic analysis

The thermoeconomic analysis was performed considering a similar parametric analysis than the previous one. Results of both thermoeconomic and unit thermoeconomic costs are presented in Fig. 7. For this analysis, as was mentioned in Section 3.4, the MS unit thermoeconomic cost was calculated under design conditions, obtaining a cost of 42.87 USD/MWh$_t$. This value was fixed for the purpose of the parametric analyses.

Under part-load operation, the thermoeconomic costs (Fig. 7.a) show that both electricity and water costs ($\dot{C}_{el}$ and $\dot{C}_w$) have a similar behavior than the exergy costs, where the $\dot{C}_{el}$ is higher as the MS mass flow rate rises, and the $\dot{C}_w$ increases until 455 kg/s and then slightly decreases until the full-load operation. Fig. 7.b illustrates that both: electric and water unit thermoeconomic costs ($c_{z\_el}$ and $c_{z\_w}$) gradually decrease with the rise of the MS mass flow rate. The largest variation of

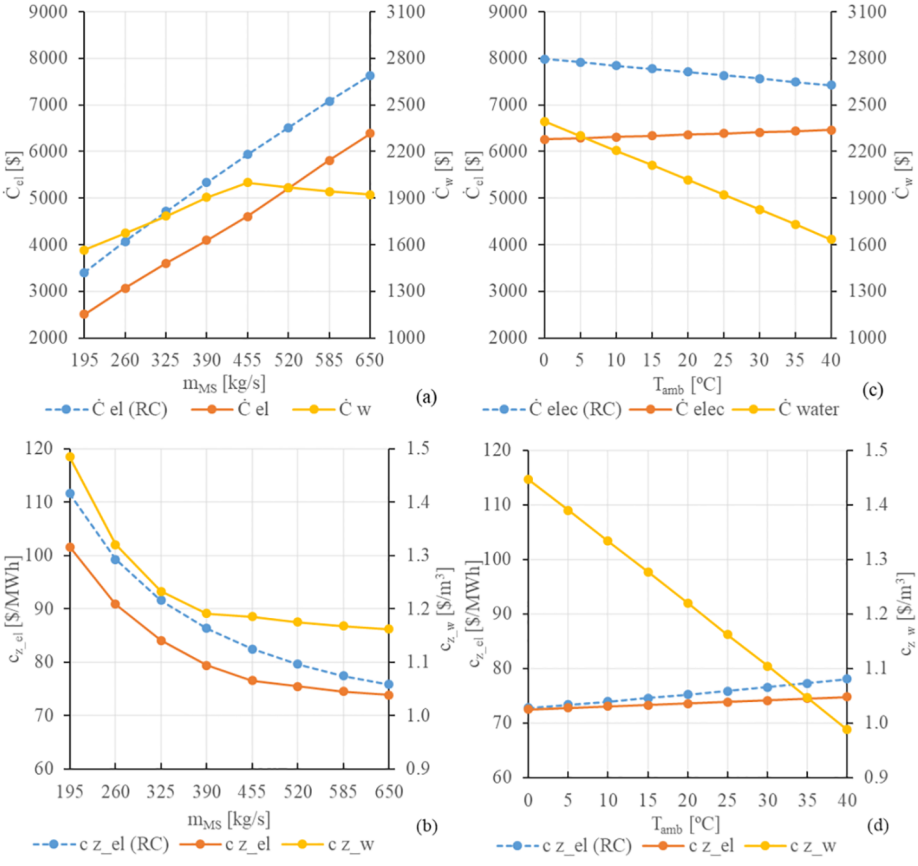


**Fig. 7.** Thermoeconomic cost and unit thermoeconomic cost of the electricity and water for (a-b) part load operation and (c-d) ambient temperature variation.

the $c_{z\_el}$ with respect to the full-load operation was 38%, while the $c_{z\_w}$ shows a maximum variation of 28%. The increases in both unit cost at part-load operation are related to the products exergy decreasing while the components cost rate remains equal. However, these results evidence that the $c_{z\_w}$ is influenced by the $c_{z\_el}$, due to the electric consumption of the MED plant and pumping system. Therefore, both unit costs are highly influenced by the part-load operation.

For the ambient temperature variation, the thermoeconomic analysis (Fig. 7.c) shows that the $\dot{C}_{el}$ has a small variation, while the $\dot{C}_{w}$ increases at lower temperatures. The results about the unit thermoeconomic cost (Fig. 7.d) shows that the $c_{z\_el}$ slightly increases at higher temperatures, while the $c_{z\_w}$ linearly rises at lower temperatures. Furthermore, the $c_{z\_el}$ shows a maximum variation of 3%, while for the $c_{z\_w}$ is about 46%. In this case, the products exergy and the component cost rate remain equal, so the costs variation are assigned by the destroyed and waste exergy flows. The increase of the $c_{z\_el}$ is associated with the steam generator and the turbines destroyed exergy contribution, but its effect is negligible, while the tendency observed for the $c_{z\_w}$ is similar to the $c_{ex\_w}$, which is affected by the increase on the waste exergy from the MED plant at lower temperatures that is completely allocated to the water cost. Thus, it can be established that the $c_{z\_w}$ is dependent on the ambient temperature. Additionally, both $\dot{C}_{el}$ and $c_{z\_el}$ of the RC + MED were lower than the $\dot{C}_{el}$ and $c_{z\_el}$ presented by the standalone RC, concluding that the MED plant coupling to a RC implies that a significant part of plant costs and the destroyed and waste exergies costs are allocated to the water, not only increasing its cost but also lowering the electricity cost.

### 4.4. MED plant sizing and location altitude impact

When analyzing an RC + MED plant, there are two variables that can significantly influence the exergetic cost and the thermoeconomic analyses: the MED plant size and the plant location's altitude. The MED plant size can be between 0 (no MED plant) and its maximum capacity, which occurs when the condenser is fully replaced. The advantages of implementing a large MED plant is the increase of freshwater production, but, the electricity consumption from the MED plant and the pumping system will also increase as well as the plant may operate more time at partial load conditions. A smaller MED plant may operate more time at nominal conditions decreasing its specific electricity consumption, but the RC will require a larger condenser. Moreover, the location's altitude can strongly influence the electric consumption of the seawater pumping system, decreasing the net electricity, but allowing to obtain freshwater at a certain altitude where it may not be available. In this section is presented the same parametric analysis of the previous section, but also varying the MED plant size and the plant location's altitude. The analysis considered an RC + MED plant with a maximum MED plant size of 60,000 $m^3$/day. Thus, six MED plant size was evaluated, from 10,000 $m^3$/day to 60,000 $m^3$/day. Also, four altitude levels were evaluated, considering also a different distance from the sea (100 m above the sea level and 20 km from the coast for the base case, and 200 m and 30 km, 500 m and 50 km and 1000 m and 100 km for the other cases respectively). Moreover, it is important to consider that the piping losses due to the distance only accounts 10% of the total in all cases, thus the altitude is the main driver that affects the seawater pumping consumption.

#### 4.4.1. Exergetic cost analysis results

Fig. 8. Presents the unit exergy cost of electricity and water for different MED plant sizes, at 100 m of altitude. In Fig. 8.a and .b it is presented the $c_{ex\_el}$ for different MS mass flow rates and ambient temperatures. Results show that the lowest values of $c_{ex\_el}$ at full-load operation are found for larger MED plant capacities (more than 50,000 $m^3$/day). Moreover, as the MS mass flow rate decreases, the $c_{ex\_el}$ of large MED pants is more sensitive to variations than smaller MED plant sizes. On the other hand, the $c_{ex\_el}$ of large MED plants slightly increases as the temperature rises, while the $c_{ex\_el}$ of smaller MED plant sizes (between 10,000 and 20,000 $m^3$/day) decreases at higher temperatures, yet, the effect of the temperature on the $c_{ex\_el}$ is not significant. From these results, it was obtained that larger MED plants imply the use of a smaller condenser, decreasing the destroyed exergy in this component. Hence, the $c_{ex\_el}$ has a lower allocation of the destroyed exergy of the plant.

Fig. 8.c and .d shows the results for the $c_{ex\_w}$ considering the same parametric analysis. These results indicate that the lowest $c_{ex\_w}$ is found also for the largest MED plant (60,000 $m^3$/day). Moreover, for smaller sizes, the $c_{ex\_w}$ increases as the MS mass flow rate is reduced. This situation occurs due to smaller MED plant sizes require larger condensers, which present higher exergy destruction increasing the turbine's exhaust steam and the electricity cost used to operate the MED plant. Conversely, the $c_{ex\_w}$ of large MED plant sizes does not change under part-load operation. This happens because of a combination of several effects. Firstly, the part-load operation of the MED plant reduces its destroyed exergy rate and the cooling seawater flow, which also decreases the electric power required to operate the P/R system. However, the specific thermal exergy of the waste streams increases. Thus, the effect of increasing the $c_{ex\_el}$ and the specific thermal exergy of the waste streams is compensated by decreasing the electricity consumption of the MED plant and the P/R system. In contrast, for every MED plant size, the $c_{ex\_w}$ increases as the ambient temperature is lower, but the $c_{ex\_w}$ of larger MED plants is less sensitive to temperature variations than the $c_{ex\_w}$ of smaller MED plants. Moreover, the increase of the $c_{ex\_w}$ by the ambient temperature is directly related to the increase of the waste exergies allocated to the water. Therefore, results indicate that

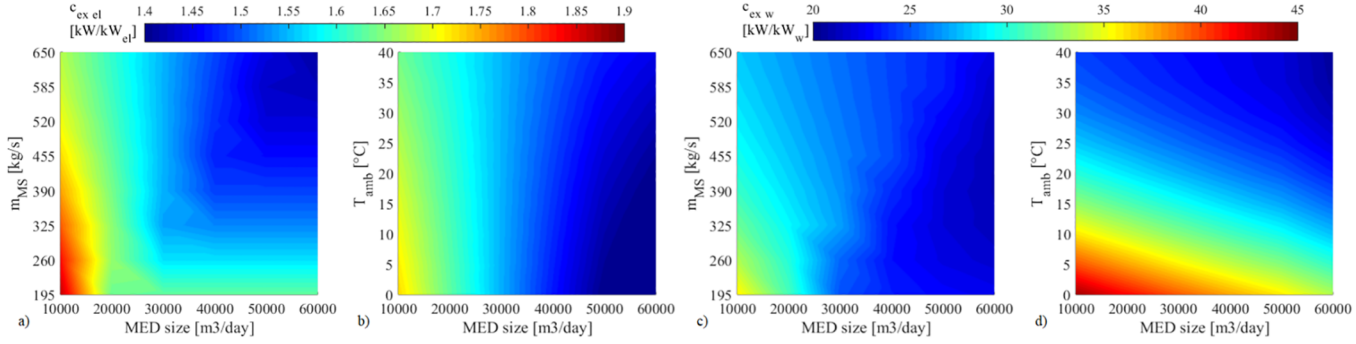


**Fig. 8.** Unit exergy cost of electricity and water for different MED sizes plant at 100 m of altitude.

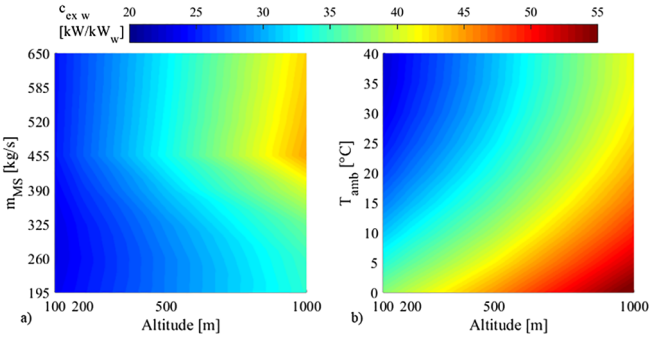


**Fig. 9.** Unit exergy cost of water for different plant location's altitudes with a MED plant of 40000 $m^3$/day.

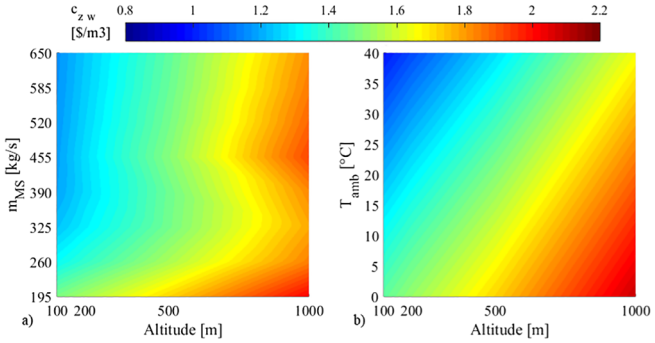


**Fig. 11.** Unit thermoeconomic cost of water for different plant location's altitudes with a MED plant of 40000 $m^3$/day.

the largest MED plant sizes achieve the lowest $c_{ex\_el}$ and $c_{ex\_w}$ under all the conditions evaluated.

The unit exergy costs were also evaluated for different plant location's altitudes, considering a fixed MED plant size of 40,000 $m^3$/day. These results are presented in Fig. 9. The main results indicate that the $c_{ex\_el}$ is not affected by the altitude since the RC operation remains equal for all altitudes. Conversely, Fig. 9.a and .b show that the $c_{ex\_w}$ significantly increases with the altitude. At part-load operation (Fig. 9.a), it is observed a slightly increase of the $c_{ex\_w}$ from 650 to 455 kg/s (70–100% of part-load operation). In this point, the 40,000 $m^3$/day MED plant achieves its maximum capacity and the ACC starts to operate or is turn off. So, the cost increase is related to the reduction of the ACC destroyed exergy and the increase of the turbine's exhaust steam flow cost. Then, for lower MS mass flow rate (under 455 kg/s), it is observed a significant decrease in the $c_{ex\_w}$. As was mentioned before, the part-load operation of the MED plant decreases the seawater steam flow lowering the electric requirements of the P/R system. This effect became more relevant for higher altitudes, decreasing the $c_{ex\_w}$. In addition, the $c_{ex\_w}$ increases due to the ambient temperature reduction at all altitudes (Fig. 9.b), which is related to the increase in the waste exergies. Therefore, the plant location's altitude has a strong impact on the $c_{ex\_w}$, and the operation conditions (MS mass flow rate and ambient temperature) have a significant influence at higher altitudes.

### 4.4.2. Thermoeconomic cost analysis results

The results of the unit thermoeconomic cost for different MED plant sizes are presented in Fig. 10. Fig. 10.a and .b show the variation of the $c_{z\_el}$ under the same parametric analysis, where the results indicate that the lowest values of the $c_{z\_el}$ are related to the largest MED sizes (more than 40,000 $m^3$/day). At larger capacities, the $c_{z\_el}$ presents a similar variation at part-load operation and it is more sensitive than at smaller capacities. Hence, for large MED plant sizes, the exergy destroyed by the throttle valve is mostly allocated to the electricity affecting the $c_{z\_el}$, while for small MED plant sizes the condenser destroys less specific exergy, which compensates the throttle valve exergy destruction. In contrast, it is observed that the $c_{z\_el}$ presents the same behavior than the one observed for the unit exergy cost when the ambient temperature varies (Fig. 8.b), showing an almost negligible effect. Thus, the main variations on the $c_{z\_el}$ are observed in part-load operation.

Fig. 10.c shows that the lowest $c_{z\_w}$ is found for the largest MED plant size (60,000 $m^3$/day) at full-load operation. However, for large MED plants, the $c_{z\_w}$ strongly increases at part-load operation, while medium MED sizes (30,000 $m^3$/day) present the lowest variation. This behavior is affected by several factors. For large MED plant, the freshwater production decreases at part-load operation, while the plant cost rate remains equal and the associated electricity cost of the pumping consumption increases. These two last factors have a greater impact on the $c_{z\_w}$, hence its value increases strongly. For medium MED plants, the part-load operation of the MED plant starts at 325–455 kg/s of MS mass flow rate, so, up to 50% part-load, the main contributors of the $c_{z\_w}$ increase are the electricity and the turbine's exhaust steam costs rise. In contrast, below 50% part-load, the $c_{z\_w}$ increase is explained mainly by the freshwater production decreasing, while the plant cost rate remains equal. However, these factors have a lower impact on the $c_{z\_w}$ in comparison to large MED plant sizes, which results in a smaller variation. Finally, for small MED plants, the freshwater production does not vary at part-load operation because the maximum MED capacity is achieved at 15–30% part-load operation. Thus, the main contributors of the increase on the $c_{z\_w}$ are the electricity and the turbine's exhaust steam costs (higher for these MED sizes), resulting in a similar behavior between the $c_{z\_w}$ and the $c_{z\_el}$. In contrast, the variation on the ambient temperature (Fig. 10.d) shows that the $c_{z\_w}$ increases as the ambient

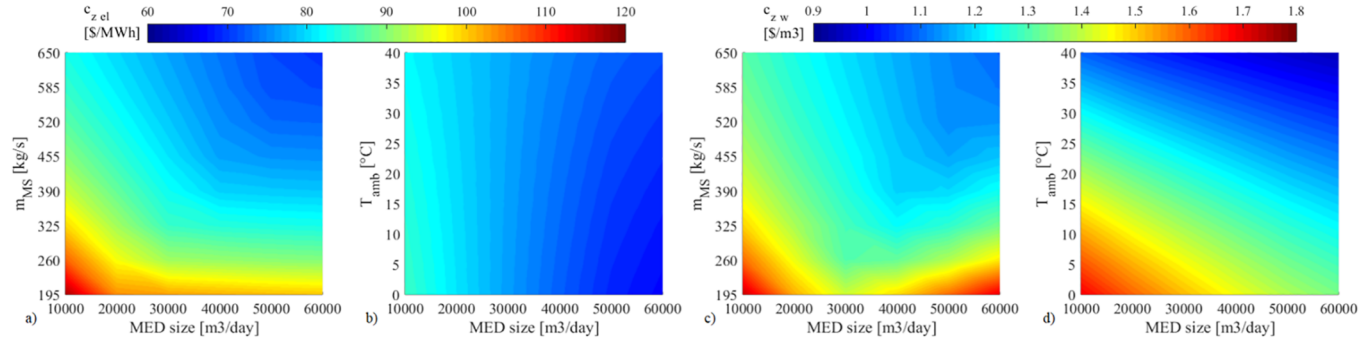


**Fig. 10.** Unit thermoeconomic cost of electricity and water for different MED sizes plant at 100 m of altitude.

**Table 3**
Composition of the electricity and water thermoeconomic cost from the MS, RC and MED plant costs.

| | Variable | $c_{z\_el}$ | $c_{z\_el\_MS}$ | $c_{z\_el\_RC}$ | $c_{z\_el\_MED}$ | $c_{z\_w}$ | $c_{z\_w\_MS}$ | $c_{z\_w\_RC}$ | $c_{z\_w\_MED}$ |
|---|---|---|---|---|---|---|---|---|---|
| | | [$/MWh] | [%] | [%] | [%] | [$/m$^3$] | [%] | [%] | [%] |
| $m_{MS}$ [kg/s] | 260 | 90.876 | 74.1% | 25.9% | 0.0% | 1.321 | 48.4% | 10.4% | 41.2% |
| | 455 | 76.620 | 82.4% | 17.6% | 0.0% | 1.186 | 57.6% | 7.9% | 34.5% |
| | 650 | 73.876 | 86.6% | 13.4% | 0.0% | 1.162 | 58.2% | 5.9% | 35.8% |
| $T_{amb}$ [°C] | 10 | 73.034 | 86.7% | 13.3% | 0.0% | 1.334 | 62.8% | 6.0% | 31.2% |
| | 25 | 73.876 | 86.6% | 13.4% | 0.0% | 1.162 | 58.2% | 5.9% | 35.8% |
| | 40 | 74.775 | 86.5% | 13.5% | 0.0% | 0.988 | 52.0% | 5.8% | 42.2% |
| MED size [m$^3$/day] | 20,000 | 79.894 | 86.3% | 13.7% | 0.0% | 1.251 | 58.9% | 6.5% | 34.6% |
| | 40,000 | 73.876 | 86.6% | 13.4% | 0.0% | 1.162 | 58.2% | 5.9% | 35.8% |
| | 60,000 | 69.702 | 86.9% | 13.1% | 0.0% | 1.095 | 55.8% | 5.2% | 39.0% |
| Altitude [m] | 100 | 73.876 | 86.6% | 13.4% | 0.0% | 1.162 | 58.2% | 5.9% | 35.8% |
| | 500 | 73.876 | 86.6% | 13.4% | 0.0% | 1.443 | 62.1% | 7.1% | 30.8% |
| | 1000 | 73.876 | 86.6% | 13.4% | 0.0% | 1.819 | 65.6% | 8.2% | 26.2% |

temperature lower, for all the scales analyzed, where the most significant variations are observed at small sizes. This variation on the $c_{z\_w}$ is related to the MED plant waste exergies. Therefore, the results from this thermoeconomic analysis indicate that the largest MED plants achieve the lowest $c_{z\_el}$ and $c_{z\_w}$, but, if the plant operates several hours at part-load, the lowest $c_{z\_w}$ would be obtained for medium MED sizes (30,000 – 40,000 m$^3$/day).

Lastly, the results of the unit thermoeconomic cost for different plant location's altitudes are presented in Fig. 11. Similar to the exergetic cost analysis, it was obtained that the $c_{z\_el}$ is not affected by the altitude of the plant, since the RC operation and the gross electricity productions remain equal. Fig. 11.a and .b show that the $c_{z\_w}$ increases significantly with the altitude. Moreover, the $c_{z\_w}$ is less sensitive to variations at higher altitudes under part-load operation. It is observed an inflection point at 455 kg/s of MS mass flow rate (70% of part-load operation), denoted as the flow rate when the ACC is activated for a 40,000 m$^3$/day MED plant size. As depicted in the exergetic cost analysis, from 650 to 455 kg/s it is observed a slight increase of the $c_{z\_w}$, due to the rise of both: the turbine's exhaust steam and the electricity cost. However, for lower MS mass flow rates (under 455 kg/s), it is observed a different behavior. From 455 to 325 kg/s (50–70% of part-load operation), the $c_{z\_w}$ tends to decrease, and then, from 325 to 195 kg/s (30–50 of part-load operation), it sharply increases. In this region, there are three main effects that contribute to such behavior. First, the electricity consumption of the P/R system decreases due to the lowering of the seawater cooling flow rate. Second, the $c_{z\_el}$ increases up to 100 $/MWh at lowest part-load operation, which strongly impacts the $c_{z\_w}$ due to the MED plant and pumping consumption. And lastly, the cost rate of the MED plant remains equal at the part-load operation while the freshwater production decreases, increasing $c_{z\_w}$. Hence, from 455 to 325 kg/s, the first effect is more relevant, but, for lower MS mass flow rates, the other two effects become more relevant. These results demonstrate that the plant cost rates have a major impact on the $c_{z\_w}$ than the destroyed exergy. Conversely, Fig. 11.b also indicates that the $c_{z\_w}$ increases as the ambient temperature are lower for all the altitudes, and it is equally sensitive for the highest elevations. This increase is related to the MED plant waste exergies that increases for lower temperatures. Finally, it is established that the altitude has a strong impact on the $c_{z\_w}$, however, several factors affect the $c_{z\_w}$ at part-load operation, which is more relevant at higher altitude.

The thermoeconomic analysis has shown that the $c_{z\_w}$ tends to be influenced by the $c_{z\_el}$. This is due to a significant part of the $c_{z\_w}$ comes from the MS and RC components cost. Table 3 shows the composition of the $c_{z\_el}$ and the $c_{z\_w}$ from the MS, the RC, and the MED plant and P/R system cost, for three different MS mass flow rates, ambient temperatures, MED plant sizes, and altitudes. In this analysis, the base case is the design configuration (650 kg/s, 25 °C, 40,000 m$^3$/day and 100 m), changing one design variable and remaining constant the other. It is observed that the $c_{z\_el}$ is mainly composed 86% by the MS cost and 14% by the RC cost (which only changes for part-load operation), while the $c_{z\_w}$ is roughly composed 36% by the MED plant cost, 58% by the MS cost and 6% by the RC cost. This composition changes significantly at part-load operation, different ambient temperatures, and location's altitudes.

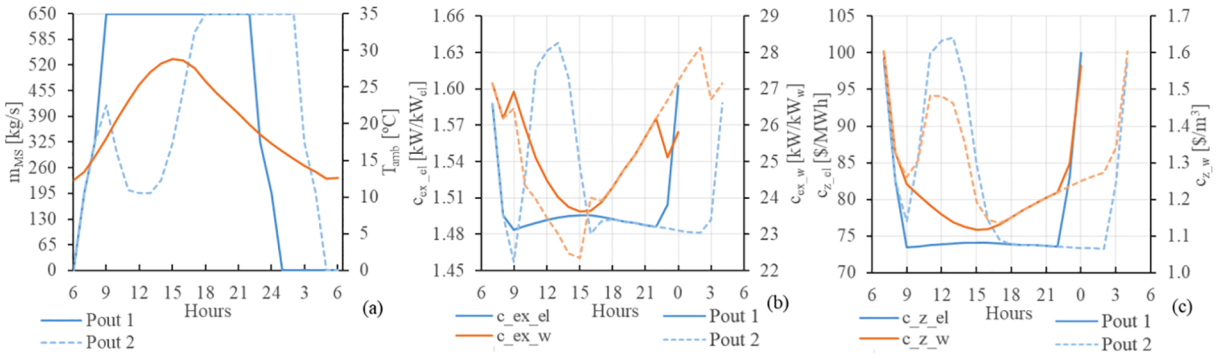


**Fig. 12.** (a) Layout of one operational day with two MS mass flow rate input, (b) unit exergy cost of electricity and water, and (c) unit thermoeconomic cost of electricity and water for one day of operation.

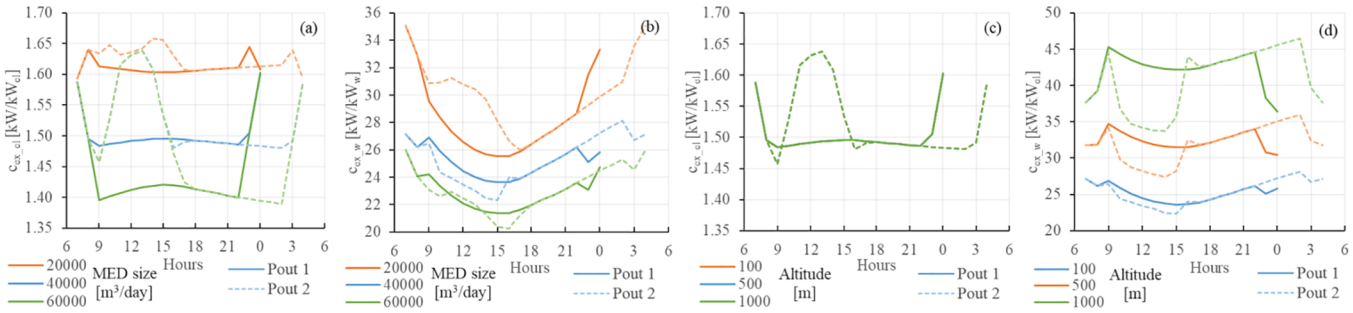


**Fig. 13.** Unit exergy cost of electricity (a, c) and water (b, d) for one operational day varying the MED plant size and the plant location's altitude.

### 4.5. Operational day performance

To integrate all the parametric analysis performed, an analysis of one operational day of the RC + MED considering the design conditions of the plant. Two power output profiles were considered, with different operation modes of an RC + MED plant coupled to a CSP plant. The first one (Pout 1) is the typical profile observed in a CSP plant, considering the ramping up and down of the plant. The second one (Pout 2) is a profile in which the CSP plant works in parallel with a PV plant, forced to operate at part-load during the day and to store more energy in the thermal energy storage enhancing the production at non-solar hours. This profile has been used by Starke et al. [49], Valenzuela et al. [18] and Zurita et al. [45], when analyzing hybrid CSP + PV plants. Fig. 12.a shows the two profiles in function of the MS mass flow rate and ambient temperature throughout the day.

Fig. 12.b and .c show the results for unit exergy cost and unit thermoeconomic cost for both output profiles, respectively. In Fig. 12.b, the $c_{ex\_el}$ presented by the Pout 1 profile remains constant during the day with a small variation, while the $c_{ex\_w}$ presents an important variation during the day, because of the temperature variation. Moreover, the $c_{ex\_el}$ developed by the Pout 2 profile presents a large increase due to the part-load operation, while the $c_{ex\_w}$ has a relevant decrease during the part-load operation. Moreover, in Mata-Torres et al. [47] it is shown a similar result, were the $c_{ex\_w}$ has an important variation, however, the main driver that changes its cost is the ambient temperature. In Fig. 12.c, the $c_{z\_el}$ remains stable throughout the day for the Pout 1 profile, while $c_{z\_w}$ has a moderate variation due to temperature variations. Besides that, the $c_{z\_el}$ observed for the Pout 2 presents a large increase of more than 25 $/MWh, while the $c_{z\_w}$ presents a significant increase at part-load operation. These results reinforce the analysis carried out in the previous section, showing that, in the exergetic cost analysis, the $c_{ex\_el}$ depends mainly on the part-load operation, while the $c_{ex\_w}$ highly depends on the ambient temperature. In contrast, in the thermoeconomic analysis, the $c_{z\_el}$ and the $c_{z\_w}$ are strongly influenced by the part-load operation, while the $c_{z\_w}$ depends moderately on the temperature.

Moreover, the MED plant size and the altitude can impact on the performance cost during the day. Fig. 13 shows the unit exergy cost results for one operational day considering three MED plants sizes and altitudes. In Fig. 13.a and .c is shown that the $c_{ex\_el}$ decreases as the MED plant size are larger, yet, it does not change with the altitude variation. For the Pout 2 profile, the large MED plant sizes present a higher increase on the $c_{ex\_el}$ at part-load operation, compared to small MED plants. In Fig. 13.b and .d it is shown that the Pout 1 profile has a variation on $c_{ex\_w}$ at the different MED plant sizes and altitudes during the day, which is related to the temperature variation. However, for the Pout 2 profile, different effects in $c_{ex\_w}$ are observed at part-load operation, on which it can be highlighted that the 40,000 $m^3$/day MED plant size and the higher altitudes cases present the largest decrease. In this case, it is noted that the $c_{ex\_el}$ is mainly influenced by the part-load operation, and the impact is higher for large MED plants, while the ambient temperature has a moderate influence on the $c_{ex\_w}$. Yet, the impact of part-load operation becomes more relevant than the ambient temperature for small MED plants and higher altitudes.

Fig. 14 shows the unit thermoeconomic cost results for one operational day considering three MED plants sizes and altitudes. In Fig. 14.a and .c, the $c_{z\_el}$ decreases as the MED plant size is larger, but it does not change with the altitude variation. Moreover, for the Pout 2 profile, the largest MED plant sizes present the largest increase in the $c_{z\_el}$ at part-load operation. In Fig. 14.b and .d, the $c_{z\_w}$ also decreases for large MED plant sizes and it increases at higher altitudes, but, the $c_{z\_w}$ in all cases has a moderate variation due to the ambient temperature. For the Pout 2 profile, the largest MED plant size presents the largest increase of the $c_{z\_w}$ at part-load operation, while at higher altitudes it is less sensitive. Thus, the $c_{z\_el}$ is strongly influenced by the part-load operation, while the $c_{z\_w}$ is mainly affected by the part-load operation, having a higher

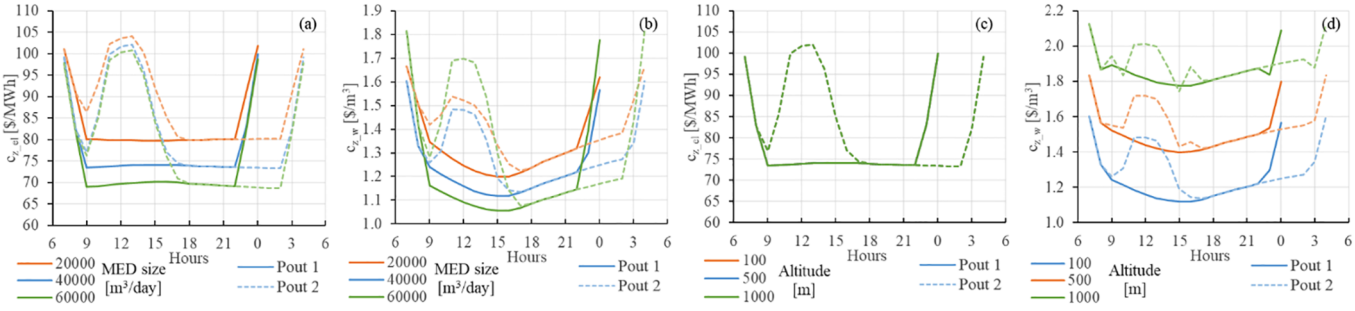


**Fig. 14.** Unit thermoeconomic cost of electricity (a, c) and water (b, d) for one operational day varying the MED plant size and the plant location's altitude.

**Table 4**
Daily production, daily unit exergy and thermoeconomic cost of the electricity and water.

| | | | Electricity | Water | $c^*_{ex\_el}$ | $c^*_{ex\_w}$ | $c^*_{z\_el}$ | $c^*_{z\_w}$ |
|---|---|---|---|---|---|---|---|---|
| | | | [MWh] | [$m^3$] | [$kW/kW_{el}$] | [$kW/kW_w$] | [$/MWh] | [$/$m^3$] |
| MED size [$m^3$/day] | Pout1 | 20,000 | 1357 | 15,069 | 1.609 | 28.43 | 81.34 | 1.33 |
| | | 40,000 | 1342 | 28,159 | 1.495 | 25.03 | 75.33 | 1.21 |
| | | 60,000 | 1335 | 38,486 | 1.423 | 22.67 | 71.46 | 1.17 |
| | Pout2 | 20,000 | 1300 | 18,707 | 1.619 | 30.02 | 84.56 | 1.41 |
| | | 40,000 | 1291 | 32,057 | 1.503 | 25.41 | 78.35 | 1.28 |
| | | 60,000 | 1288 | 40,272 | 1.447 | 23.14 | 75.15 | 1.28 |
| Altitude [m] | Pout1 | 100 | 1342 | 28,159 | 1.495 | 25.03 | 75.33 | 1.21 |
| | | 500 | 1252 | 28,159 | 1.495 | 32.42 | 75.31 | 1.49 |
| | | 1000 | 1130 | 28,159 | 1.495 | 42.36 | 75.28 | 1.85 |
| | Pout2 | 100 | 1291 | 32,057 | 1.503 | 25.41 | 78.35 | 1.28 |
| | | 500 | 1196 | 32,057 | 1.503 | 32.27 | 78.30 | 1.55 |
| | | 1000 | 1070 | 32,057 | 1.503 | 41.40 | 78.25 | 1.89 |

impact for larger MED plants and at lower altitudes. The ambient temperature has a minor impact being less sensitive at higher altitudes.

The exergetic cost and thermoeconomic analysis results have shown that the part-load operation during the day implies a variation on the unit cost. The daily production, daily unit exergy cost ($c^*_{ex}$) and daily thermoeconomic cost ($c^*_z$) of electricity and water of each one of the cases were calculated and summarized in Table 4. Such results show that the net electricity production for the Pout 2 profile decreases compared to the operation mode described by the Pout 1 profile, while the water production increases. However, the $c^*_{ex}$ and $c^*_z$ observed under the Pout 1 operation mode are lower than the cost for the Pout 2 profile, in almost all the cases reported. The only exception was for the altitude of 500 m and 1000 m, where $c^*_{ex\_w}$ for the Pout 2 profile is lower than the cost observed for Pout 1 profile. It can be concluded that the operation at part-load of the RC + MED plant for some hours during the day may provide more water production but at a moderate higher unit exergy and thermoeconomic cost. Also, results illustrate that the largest MED plant size achieves the lowest $c^*_{ex}$ and $c^*_z$, which indicate that it constitutes the best configuration. Finally, it is shown throughout all the analyses, that the effect of the altitude is allocated to the water, but for a higher altitude, the differences between $c^*_{z\_w}$ for the Pout 1 and the Pout 2 profile are smaller; thus, it is less sensitive to part-load operation from the thermoeconomic point of view.

## 5. Conclusions

A Rankine Cycle coupled to a Multi-Effect Distillation (RC + MED) plant was studied to analyze the exergy cost formation, the exergy destruction and the thermoeconomic cost of the final products: electricity and freshwater. For this purpose, a detailed RC + MED model was performed, considering a high-disaggregation level, in which the solar molten salts drive the RC. The analysis was performed varying the molten salts mass flow rate, allowing to assess the performance in part-load operation, the ambient temperature, the MED plant size, and the location plant's altitude. Finally, a detailed analysis of an operational day for the RC + MED considering two power output profiles (where one was the typical profile observed in a CSP plant, and the other was a profile in which the CSP plant works in parallel with a PV plant) was carried out. Those analyses allowed to identify the impact of these operational conditions on the exergy performance, as well as the exergy and thermoeconomic costs of the final products.

Results for the exergy performance show that coupling the MED plant to the RC increases the exergy destruction on the dissipative components of the plant (the MED and the ACC), and it reduces the exergetic efficiency of the system. Additionally, it was found that the MED plant is the second component with the highest contribution to the exergy destruction of the plant, reaching 21.7% of the total; while the chemical exergy of the freshwater has a small value compared to other outputs. The parametric analyses indicate that the throttle valve increases its destroyed exergy contribution under the plant part-load operation, and the wasted exergy rises as the ambient temperature is lower.

The exergetic cost analysis showed that the part-load operation has a more significant influence in the exergy cost of electricity than on the cost of water, while the latter is highly dependent on the ambient temperature since it increases its value at lower temperatures. This behavior evidences that the exergy destroyed by the throttle valve is mainly allocated to the electricity, while the increase in exergy waste is allocated to the freshwater produced. In contrast, the results from the thermoeconomic analysis evidenced that both unit costs are highly influenced by the part-load operation, while the effect of the ambient temperature on the unit thermoeconomic cost of electricity is almost negligible but is moderately significant on the cost of water. This reflects that the electric consumption by the MED and the P/R system becomes more relevant in the cost formation process of the water.

Regarding the parametric analysis of the MED plant size and the plant location's altitude, the exergetic cost analysis showed that the largest MED plant sizes (above 50,000 $m^3$/day) achieve the lowest unit exergy cost of electricity and water under all the conditions evaluated. Moreover, results indicate that the variation of the plant location's altitude has a strong impact on unit exergy cost of water increasing its value with the altitude, in which the operational conditions (molten salts mass flow rate and ambient temperature) have a more significant influence at higher altitudes. The thermoeconomic cost results showed that the largest MED plant sizes achieved the lowest unit thermoeconomic cost of electricity and water. However, the lowest water cost could be obtained for medium MED plant sizes (30,000–40,000 $m^3$/day) if the plant operates several hours at part-load conditions. In addition, it was found that the altitude has a strong impact on the unit thermoeconomic cost of water, increasing its value for higher location due to the pumping energy requirements. Lastly, it was determined that the unit thermoeconomic cost of electricity is mainly composed 86% by the molten salts cost and 14% by the RC cost, while the unit

thermoeconomic cost of water is roughly composed 58% by the molten salts cost, 6% by the RC cost and 36% by the MED plant and P/R system cost.

The analysis of the operational day of the RC + MED indicates that unit exergy cost of electricity mainly depends on the part-load operation, being more sensitive to increase with large MED plant sizes; while the unit exergy cost of water is moderately influenced by the ambient temperature. In contrast, the unit thermoeconomic results showed that both, electricity and water costs, are strongly influenced by the part-load operation, in which the unit water cost present higher effect for large MED plant sizes and lower altitudes, while the unit water cost is moderate dependent on the temperature, being less sensitive at higher altitudes. Lastly, the analysis showed that the part-load operation of the RC + MED plant during the day may provide more water production, but at moderate higher exergy and thermoeconomic cost.

The result of this work demonstrated that the exergetic cost analysis considers the allocation of the destroyed and waste exergy on the products, in which the results show that the part-load operation is the most relevant factor and the temperature has an important impact only in the water cost. Whereas, in the thermoeconomic cost analysis, the cost of the components has a higher impact than the destroyed and waste exergy effects, obtaining that the part-load operation is the main factor that affects both costs, and the ambient temperature as a slightly effect only in the water cost. Hence, the operation of these plants should be conceived as full-load most of the time. Moreover, larger MED plants configuration (between the 80–100% of the maximum capacity) present the lowest exergy and thermoeconomic costs of electric and water. However, these configurations could present a technical challenge at part-load operation because the MED plant has to ensure the cooling requirements by the RC. In contrast, the location altitude has non-impact on the electricity cost, but it has a high influence in the water cost, so locations near of the cost (low altitude) could achieve lower water costs. Nevertheless, these locations may present lower direct normal irradiation resource that would decrease the energy available for the power cycle in a CSP plant. Therefore, in further works, it is recommended to include CSP components and the solar resource variability of the location in the analyses, which would allow to assess the cost formation of the products from the sun exergy and to evaluate other solar technologies integration such as the hybridization into a CSP + PV concept.

## Declaration of interests

None.

## Acknowledgments

The authors appreciate the support from CONICYT/FONDAP 15110019 “Solar Energy Research Center”- SERC-Chile. Also, authors gratefully acknowledge the support from Fraunhofer Chile Research – Center of Solar Energy Technologies by the Corfo project 13CEI2-21803. C. Mata-Torres would like to the acknowledge doctoral scholarship from CONICYT PFCHA/Doctorado Nacional 2018/21181537. Also, A. Zurita would like to acknowledge the Pontificia Universidad Católica de Chile VRI doctoral scholarship support.

## Appendix A.1. Details of the auxiliary equations used to the exergetic cost analysis

The auxiliary equations were separated into three main groups: RC equations, MED plant equations, and P/R system equations. The RC equations summary are the following:

- The input exergy of the hot MS is equal to its exergy cost ($C_i$).
- $C_i$ of all MS streams are equal to 1.
- $C_i$ of the air output from the ACC is equal to 0.
- $c_{ex\_i}$ of the turbine inlet steam is equal to the $c_{ex\_j}$ of the turbine outlet steam
- $c_{ex\_i}$ of the pump inlet stream is equal to the $c_{ex\_j}$ of the pump outlet stream
- $c_{ex\_i}$ of the hot inlet steam of the CFWH heater is equal to the $c_{ex\_j}$ of the hot outlet steam of the CFWH heater
- $c_{ex\_i}$ of all extractions of the same turbine have the same value.
- $c_{ex\_i}$ of the air inlet of the ACC is equal to the $c_{ex\_j}$ of the air outlet from the ACC.
- $c_{ex\_i}$ of the net electricity produced is equal to the $c_{ex\_j}$ of the total pump power consumed.
- $c_{ex\_i}$ of the net electricity produced is equal to the $c_{ex\_j}$ of the ACC electric power consumed.

For the MED plant, it was selected a disaggregation level that analyzes each effect separately (12 components). In Fig. 15 shows the first, an intermediate and the final effect of the plant, with the considered streams. For the effects 1 to 11, six outputs were defined: the physical and chemical exergy of the vapor distillate stream ($vd_{ph,i}$ and $vd_{ch,i}$), of the condensate distillate stream ($cd_{ph,i}$ and $cd_{ch,i}$), and of the brine stream ($b_{ph,i}$ and $b_{ch,i}$), and one input: the physical exergy of the feed-seawater ($f_i$), which are the inputs and the output of the following effect. In addition, in the first effect was considered the input steam ($st_{in}$) from the turbine exhaust and output condensate ($st_{out}$) that goes to the power cycle pump. Also, it was included a desuperheater that decreases the enthalpy of the $st_{in}$ to the saturated vapor enthalpy, if this stream is in the superheated state, with a fraction of the condensate distillate of the last effect. Thus, it was considered the distillate desuperheater stream ($dsh_1$) as an input of the first effect. For the last effect, it was considered one additional input: the physical exergy of the condenser input seawater ($s_{in\_2}$) and seven output: the physical exergy of the cooling water seawater stream ($s_{cw}$) used to condensate all the distillate in the last effect, and the physical and chemical exergy of the brine ($b_{ph,12}$ and $b_{ch,12}$), the physical and chemical exergy of the condensate distillate ($cd_{ph,12}$ and $cd_{ch,12}$) and the physical and chemical exergy of the distillate used in the desuperheater ($dsh_{ph,1}$ and $dsh_{ch,1}$). In Fig. 15, the $b_i$, $vd_i$, $cd_i$ and $dsh_1$ streams consider separately the physical and the chemical exergy. Finally, for the MED plant, it was defined as the electric consumption of the MED plant ($P_{MED\_i}$), which was divided by the 12 effects as an input for each MED component. For these streams, the MED auxiliary equations are the following [26]:

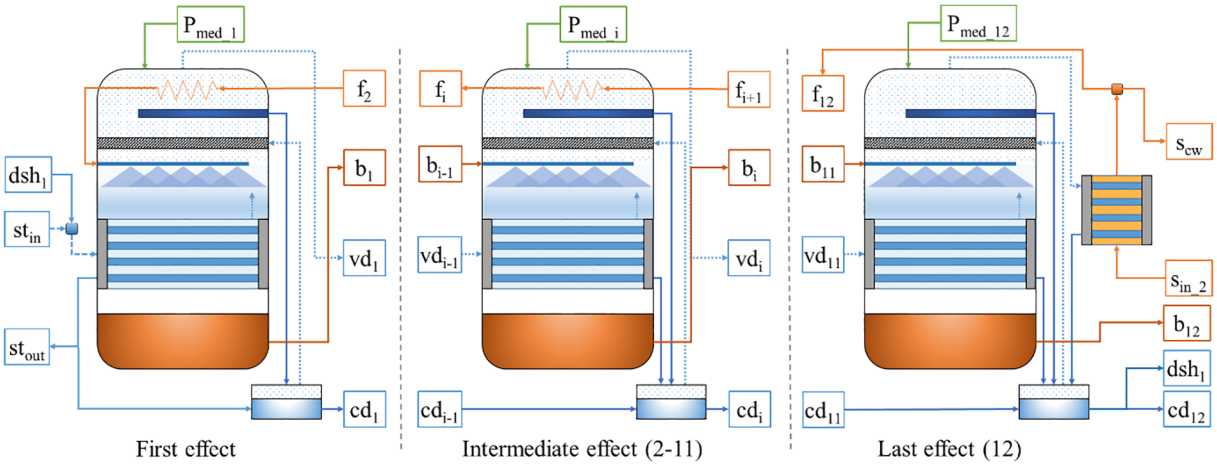


**Fig. 15.** MED plant components (first effect, intermediate effect, and last effect) with the streams considered.

- $C_i$ of the $b_{ch,i}$ of every effect is equal to 0.
- $C_i$ of the $cd_{ph,12}$ is equal to 0.
- $c_{ex\_i}$ of the $vd_{ph,i}$ is equal to the $c_{ex\_j}$ of the $cd_{ph,i}$ for effect from 1 to 11.
- $c_{ex\_i}$ of the $vd_{ch,i}$ is equal to the $c_{ex\_j}$ of the $cd_{ch,i}$ for effects from 1 to 11.
- $c_{ex\_i}$ of the $vd_{ph,i}$ is equal to the $c_{ex\_j}$ of the $vd_{ch,i}$ for effects from 1 to 11.
- $c_{ex\_i}$ of the $b_{ph,i}$ is equal to the $c_{ex\_j}$ of the $b_{ph,i+1}$ of the following effect.
- $c_{ex\_i}$ of the $cd_{ph,1}$ of the first effect is equal to the $c_{ex\_j}$ of the $b_{ph,1}$ of the first effect.
- $c_{ex\_i}$ of the $f_{12}$ of the last effect is equal to the $c_{ex\_j}$ of the $s_{cw}$.
- $c_{ex\_i}$ of the $st_{in}$ and $st_{out}$ that power the MED plant are equal.
- $c_{ex\_i}$ of the $dsh_{1,ch}$ is equal to the $c_{ex\_j}$ of the $cd_{ch,12}$.
- $c_{ex\_i}$ of the $dsh_{1,ch}$ is equal to the $c_{ex\_j}$ of the $dsh_{1,ph}$.

For the P/R system, it was considered 4 components: a brine mixer, where the output brine from the 12th effect ($b_{12}$) is mixed with the resultant $s_{cw}$, resulting in the mixed brine stream ($b_{mix1}$), the pumping system (includes the pipeline and the pump), the recovery system (it includes the pipeline and the turbine) and a net MED plant electric node where is calculated the required electricity for the MED plant operation. Also, it was considering the following streams: the physical exergy of pumping input seawater ($s_{in\_1}$), the physical and chemical exergy of the mixed brine ($b_{ph\_mix1}$ and $b_{ch\_mix1}$), the physical and chemical exergy of the mixed brine at sea level ($b_{ph\_mix2}$ and $b_{ch\_mix2}$) after the energy recovery system, the power output of the turbine ($P_{tur\_MED}$), the power required by the pump ($P_{p\_MED}$) and the net electricity required by the MED plant and P/R system ($P_{MED\_t}$). For these streams, the P/D system equations are the following:

- $C_i$ of the $s_{in\_1}$ is equal to its exergy cost.
- $C_i$ of the $b_{ch\_mix1}$ is equal to 0.
- $C_i$ of the $b_{ch\_mix2}$ is equal to 0.
- $c_{ex\_i}$ of the $b_{ph\_mix1}$ is equal to the $c_{ex\_j}$ of the $b_{ph\_mix2}$.
- $c_{ex\_i}$ of the $P_{p\_MED}$ is equal to the $c_{ex\_j}$ of the power required by the MED plant.
- $c_{ex\_i}$ of the $P_{MED\_t}$ is equal to the $c_{ex\_j}$ of the net electricity produced.

Finally, the $b_{ph\_mix2}$ is a stream that is considered a waste, however, it cost is related to the unit exergy cost of some streams that are resources or products of different components. For this issue, Piacentino [26] proposes to divide the exergy costs corresponding to this stream between the effect of MED plant, in order to share as an additional input cost in all the components (each effect) that have contributed to generating the residue.

## Appendix A.2. Details of the cost function of the plant components

Table 5.

**Table 5**
Cost function correlation for each plant component [26,42–44,50].

| Component | TCI equation | Observation |
|---|---|---|
| Steam generator | $TCI_{boi} = 208582\frac{\$}{kgs}\dot{m}_{sg}{}^{0.8}e^{\left(\frac{Pr_{\dot{v}}-28}{150}\right)}F_{an}F_{at}F_{sgrh}F_{an} = 1 + \left(\frac{1-0.95}{1-\eta_{boi}}\right)^7 F_{at} = 1 + 5e^{\left(\frac{T_1-593}{10.42}\right)}F_{sgrh}$ $= 1 + \frac{Tsg_{out} - Tsg_{in}}{Tsg_{out}} + \left(\frac{\dot{m}_{sg}}{\dot{m}_{rh}}\right)\frac{(Trh_{out} - Trh_{in})}{Trh_{out}}TCI_{sg} = (1 - f_{rh})TCI_{boi}f_{rh} = 0.12$ | $\dot{m}_{sg}$ is the design steam mass flow rate of the steam generator, $Pr_{\dot{v}}$ is the steam generator pressure in MPa, $T_1$ is output temperature in °C, $\eta_{boi}$ is the thermodynamic efficiency of the boiler, $\dot{m}_{rh}$ is the design steam mass flow rate of the reheater, $T_{sg}$ is the input or output temperature of the steam at the steam generator and $T_{rh}$ is the input or output temperature of the reheater. |
| Re-heater | $TCI_{rh} = f_{rh}Z_{boi}$ | $f_{rh}$ is the ratio of the investment cost of the reheater to the investment cost of the boiler. |
| Turbine | $TCI_{st} = 3880.5\frac{\$}{kW^{-0.7}}P_{st}{}^{0.7}\left[1 + \left(\frac{0.05}{1-\eta_{st}}\right)^3\right]\left[1 + 5e^{\left(\frac{T_a-886}{10.42}\right)}\right]$ | $P_{st}$ is the power output of the turbine, $\eta_{st}$ is the isentropic efficiency of the turbine and $T_a$ is the input steam temperature. |
| Pump | $TCI_{pump} = 705.48\frac{\$}{kgs}P_{pump}{}^{0.71}\left(1 + \frac{0.2}{1-\eta_{pump}}\right)$ | $P_{pump}$ is the power of the pump and $\eta_{PUMP}$ is the isentropic efficiency of the pump. |
| Condenser | $TCI_{cond} = \left(\frac{1}{T_o e}\right)\left\{217\left[0.247 + \left(\frac{1}{3.24V_W{}^{0.8}}\right)\right]\ln\left(\frac{1}{1-e}\right) + 138\right\}\left(\frac{1}{1-\eta_{cond}}\right)Se$ $= \frac{T_{wo} - T_{wi}}{T_{in} - T_{wo}}$; $\eta_{cond} = \frac{T_o(s_{in} - s_{out})}{h_{in} - h_{out}}$ | $T_o$ is the ambient temperature in °C, $V_w$ is the velocity of the cooling water in the condenser (m/s), $T_{wo}$, $T_{wi}$ and $T_{in}$ are the temperature of the outlet cooling air, inlet cooling air and inlet steam in the condenser, respectively in °C, $e$ the thermal effectiveness, $\eta_{cond}$ the efficiency of the condenser, and $S$ is the negentropy in kW. |
| Deaerator | $TCI_{dea} = 145315\frac{\$}{kW^{-0.7}}\dot{m}_{water}{}^{0.7}$ | $\dot{m}_{water}$ is the output water mass flow rate of the deaerator. |
| Closed FWH | $TCI_{cfwh,i} = (1000 \bullet 0.02 \bullet 3.3)Q\left(\frac{1}{T_{td,i}+a}\right)^{0.1}(10\Delta Pr_t)^{-0.08}(10\Delta Pr_{\dot{s}})^{-0.04}$ $a = 6$ for high pressure CFWH and $a = 4$ for low pressure CFWH | $Q$ is the amount of heat transfer in the CFWH in kW; $T_{td}$ is the difference between the saturated temperature of the steam extracted from the turbine and the temperature of the outlet feed in the CFWH in °C; $\Delta Pr_t$ and $\Delta Pr_{\dot{s}}$ are the pressure drop of the feed water and the extraction steam in the CFWH, respectively in MPa. |
| Generator | $TCI_{gen} = 60P_{gen}{}^{0.95}$ | $P_{gen}$ is the electrical power output of the generator. |
| MED plant | $TCI_{med} = 300A_{total}{}^{0.95}TCI_{effect,1} = Z_{med}\frac{1.4}{(1.4 + (N_{effect} - 2) + 1.1)}$ (First effect)<br>$TCI_{effect,i} = Z_{med}\frac{1}{(1.4 + (N_{effect} - 2) + 1.1)}$ (Intermediate effects)<br>$TCI_{effect,12} = Z_{med}\frac{1.1}{(1.4 + (N_{effect} - 2) + 1.1)}$ (Last effect with MED condenser) | $A_{total}$ is the surface area of the evaporator and preheater at all the effects and the condenser in $m^2$. The disaggregation of the MED cost considered that the first effect has a 40% higher cost and the last effect with the down condenser has a 10% higher cost than other effects. |
| Piping | $TCI_{pipe} = 50000\frac{\$}{km}L_{pipe}$ | $L_{pipe}$ is the length of the pipe that goes from the sea to the plant location. For this work, 60% of this cost was allocated to the seawater pumping system and 40% to the energy recovery system. |

## References


[1] IRENA, IEA-ETSAP. Water Desalination Using Renewable Energy. 2012.
[2] Shenvi SS, Isloor AM, Ismail AF. A review on RO membrane technology: developments and challenges. Desalination 2015;368:10–26. https://doi.org/10.1016/j.desal.2014.12.042.
[3] Mokhtari H, Sepahvand M, fasihfar A. Thermoeconomic and exergy analysis in using hybrid systems (GT + MED + RO) for desalination of brackish water in Persian Gulf. Desalination 2016;399:1–15. https://doi.org/10.1016/j.desal.2016.07.044.
[4] Abdelkareem MA, El Haj Assad M, Sayed ET, Soudan B. Recent progress in the use of renewable energy sources to power water desalination plants. Desalination 2018;435:97–113. https://doi.org/10.1016/j.desal.2017.11.018.
[5] Al-Karaghouli A, Kazmerski LL. Energy consumption and water production cost of conventional and renewable-energy-powered desalination processes. Renew Sustain Energy Rev 2013;24:343–56. https://doi.org/10.1016/j.rser.2012.12.064.
[6] Shakib SE, Amidpour M, Aghanajafi C. A new approach for process optimization of a METVC desalination system. Desalin Water Treat 2012;37:84–96. https://doi.org/10.1080/19443994.2012.661258.
[7] Gabriel KJ, Linke P, El-Halwagi MM. Optimization of multi-effect distillation process using a linear enthalpy model. Desalination 2015;365:261–76. https://doi.org/10.1016/j.desal.2015.03.011.
[8] Carballo JA, Bonilla J, Roca L, De la Calle A, Palenzuela P, Alarcón-Padilla DC. Optimal operating conditions analysis for a multi-effect distillation plant according to energetic and exergetic criteria. Desalination 2018;435:70–6. https://doi.org/10.1016/j.desal.2017.12.013.
[9] Elsayed ML, Mesalhy O, Mohammed RH, Chow LC. Transient performance of MED processes with different feed configurations. Desalination 2018;438:37–53. https://doi.org/10.1016/j.desal.2018.03.016.
[10] Uche J, Serra L, Valero A. Thermoeconomic optimization of a dual-purpose power and desalination plant. Desalination 2001;136:147–58. https://doi.org/10.1016/S0011-9164(01)00177-1.
[11] Khoshgoftar Manesh MH, Ghalami H, Amidpour M, Hamedi MH. Optimal coupling of site utility steam network with MED-RO desalination through total site analysis and exergoeconomic optimization. Desalination 2013;316:42–52. https://doi.org/10.1016/j.desal.2013.01.022.
[12] Iaquaniello G, Salladini A, Mari A, Mabrouk AA, Fath HES. Concentrating solar power (CSP) system integrated with MED-RO hybrid desalination. Desalination 2014;336:121–8. https://doi.org/10.1016/j.desal.2013.12.030.
[13] Blanco J, Palenzuela P, Alarcón-Padilla D, Zaragoza G, Ibarra M. Preliminary thermoeconomic analysis of combined parabolic trough solar power and desalination plant in port Safaga (Egypt). Desalin Water Treat 2013;51:1887–99. https://doi.org/10.1080/19443994.2012.703388.
[14] Casimiro S, Cardoso J, Ioakimidis C, Farinha Mendes J, Mineo C, Cipollina A. MED parallel system powered by concentrating solar power (CSP). Model and case study: Trapani, Sicily. Desalin Water Treat 2014;3994:1–14. https://doi.org/10.1080/19443994.2014.940222.
[15] Palenzuela P, Alarcón-Padilla DC, Zaragoza G. Large-scale solar desalination by combination with CSP: techno-economic analysis of different options for the Mediterranean Sea and the Arabian Gulf. Desalination 2015;366:130–8. https://doi.org/10.1016/j.desal.2014.12.037.
[16] Palenzuela P, Zaragoza G, Alarcón-Padilla DC. Characterisation of the coupling of multi-effect distillation plants to concentrating solar power plants. Energy 2015;82:986–95. https://doi.org/10.1016/j.energy.2015.01.109.
[17] Mata-Torres C, Escobar RA, Cardemil JM, Simsek Y, Matute JA. Solar polygeneration for electricity production and desalination: case studies in Venezuela and northern Chile. Renew Energy 2017;101:387–98. https://doi.org/10.1016/j.renene.2016.08.068.
[18] Valenzuela C, Mata-Torres C, Cardemil JM, Escobar RA. CSP + PV hybrid solar plants for power and water cogeneration in northern Chile. Sol Energy 2017;157:713–26. https://doi.org/10.1016/j.solener.2017.08.081.
[19] Wang Y, Lior N. Fuel allocation in a combined steam-injected gas turbine and thermal seawater desalination system. Desalination 2007;214:306–26. https://doi.org/10.1016/j.desal.2007.01.001.
[20] Leiva-Illanes R, Escobar R, Cardemil JM, Alarcón-Padilla D-C. Comparison of the levelized cost and thermoeconomic methodologies – cost allocation in a solar polygeneration plant to produce power, desalted water, cooling and process heat. Energy Convers Manage 2018;168:215–29. https://doi.org/10.1016/j.enconman.2018.04.107.
[21] Ortega-Delgado B, Garcia-Rodriguez L, Alarcón-Padilla D-C. Thermoeconomic comparison of integrating seawater desalination processes in a concentrating solar power plant of 5 MWe. Desalination 2016;392:102–17. https://doi.org/10.1016/j.desal.2016.03.016.
[22] Kouta A, Al-Sulaiman F, Atif M, Bin Marshad S. Entropy, exergy, and cost analyses of solar driven cogeneration systems using supercritical CO2Brayton cycles and MEE-TVC desalination system. Energy Convers Manage 2016;115:253–64. https://doi.org/10.1016/j.enconman.2016.02.021.
[23] Leiva-Illanes R, Escobar R, Cardemil JM, Alarcón-Padilla D-C. Thermoeconomic assessment of a solar polygeneration plant for electricity, water, cooling and heating in high direct normal irradiation conditions. Energy Convers Manage 2017;151:538–52. https://doi.org/10.1016/j.enconman.2017.09.002.
[24] Wellmann J, Meyer-Kahlen B, Morosuk T. Exergoeconomic evaluation of a CSP plant in combination with a desalination unit. Renew Energy 2017;128:586–602. https://doi.org/10.1016/j.renene.2017.11.070.
[25] Askari IB, Ameri M, Calise F. Energy, exergy and exergo-economic analysis of different water desalination technologies powered by Linear Fresnel solar field. Desalination 2018;425:37–67. https://doi.org/10.1016/j.desal.2017.10.008.
[26] Piacentino A. Application of advanced thermodynamics, thermoeconomics and exergy costing to a Multiple Effect Distillation plant: In-depth analysis of cost formation process. Desalination 2015;371:88–103. https://doi.org/10.1016/j.desal.2015.06.008.
[27] Catrini P, Cipollina A, Micale G, Piacentino A, Tamburini A. Exergy analysis and thermoeconomic cost accounting of a Combined Heat and Power steam cycle integrated with a Multi Effect Distillation-Thermal Vapour Compression desalination plant. Energy Convers Manage 2017;149:950–65. https://doi.org/10.1016/j.enconman.2017.04.032.
[28] Leiva-Illanes R, Escobar R, Cardemil JM, Alarcón-Padilla D-C, Uche J, Martínez A. Exergy cost assessment of CSP driven multi-generation schemes: integrating seawater desalination, refrigeration, and process heat plants. Energy Convers Manage 2019;179:249–69. https://doi.org/10.1016/j.enconman.2018.10.050.
[29] Patnode AM. Simulation and performance evaluation of parabolic trough solar power plants. Univ Wisconsin-Madison 2006:5–271.
[30] Palenzuela P, Alarcón-Padilla D-C, Zaragoza G. Concentrating solar power and desalination plants: engineering and economics of coupling multi-effect distillation and solar plants Springer International Publishing; 2015. https://doi.org/10.1007/978-3-319-20535-9.
[31] Ortega-Delgado B, Palenzuela P, Alarcón Padilla D-C. Parametric study of a multi-effect distillation plant with thermal vapor compression for its integration into a Rankine cycle power block. Desalination 2016;394:18–29. https://doi.org/10.1016/j.desal.2016.04.020.
[32] Ortega-Delgado B, García-Rodríguez L, Alarcón-Padilla D-C. Opportunities of improvement of the MED seawater desalination process by pretreatments allowing high-temperature operation. Desalin Water Treat 2017;97:94–108. https://doi.org/10.5004/dwt.2017.21679.
[33] El-Dessouky HT, Ettouney HM. Fundamentals of Salt Water. Desalination 2002. https://doi.org/10.1016/B978-044450810-2/50008-7.
[34] Ortega-Delgado B, Cornali M, Palenzuela P, Alarcón-Padilla DC. Operational analysis of the coupling between a multi-effect distillation unit with thermal vapor compression and a Rankine cycle power block using variable nozzle thermocompressors. Appl Energy 2017;204:690–701. https://doi.org/10.1016/j.apenergy.2017.07.062.
[35] Cipollina A, Micale G, Rizzuti L. Seawater Desalination. Conventional and Renewable Energy Processes. Springer; 2009.
[36] Bejan A, Tsatsaronis G, Moran M. Therm Des Optim 1995:560.
[37] Dinçer I, Rosen M. EXERGY: energy, environment and sustainable development. Elsevier Science; 2012.
[38] Sharqawy MH, Lienhard VJH, Zubair SM. On exergy calculations of seawater with applications in desalination systems. Int J Therm Sci 2011;50:187–96. https://doi.org/10.1016/j.ijthermalsci.2010.09.013.
[39] Sharqawy MH, Zubair SM, Lienhard JH. Second law analysis of reverse osmosis desalination plants: an alternative design using pressure retarded osmosis. Energy 2011;36:6617–26. https://doi.org/10.1016/j.energy.2011.08.056.
[40] Gómez-Hernández J, González-Gómez PA, Briongos JV, Santana D. Influence of the steam generator on the exergetic and exergoeconomic analysis of solar tower plants. Energy 2018;145:313–28. https://doi.org/10.1016/j.energy.2017.12.129.
[41] Tsatsaronis G. Thermoeconomic analysis and optimization of energy systems. Prog Energy Combust Sci 1993;19:227–57. https://doi.org/10.1016/0360-1285(93)90016-8.
[42] Adibhatla S, Kaushik SC. Exergy and thermoeconomic analyses of 500 MWe sub critical thermal power plant with solar aided feed water heating. Appl Therm Eng 2017;123:340–52. https://doi.org/10.1016/j.applthermaleng.2017.05.099.
[43] Xiong J, Zhao H, Zhang C, Zheng C, Luh PB. Thermoeconomic operation optimization of a coal-fired power plant. Energy 2012;42:486–96. https://doi.org/10.1016/j.energy.2012.03.020.
[44] Ameri M, Ahmadi P, Hamidi A. Energy, exergy and exergoecnomic analysis of a steam power plant: a case study. Int J Energy Res 2009;33:499–512. https://doi.org/10.1002/er.1495.
[45] Zurita A, Mata-Torres C, Valenzuela C, Felbol C, Cardemil JM, Guzmán AM, et al. Techno-economic evaluation of a hybrid CSP + PV plant integrated with thermal energy storage and a large-scale battery energy storage system for base generation. Sol Energy 2018;173:1262–77. https://doi.org/10.1016/j.solener.2018.08.061.
[46] Lilliestam J, Pitz-Paal R. Concentrating solar power for less than USD 0.07 per kWh: finally the breakthrough? Renew Energy Focus 2018;26:17–21. https://doi.org/10.1016/j.ref.2018.06.002.
[47] Mata-Torres C, Zurita A, Cardemil JM, Escobar RA. Exergy cost analysis of a CSP-Rankine Cycle coupled with a MED plant considering time- varying conditions and part-load operation. 31th Int Conf. Effic. Cost, Optim. Simul. Environ. Impact Energy Syst. ECOS 2018. 2018.
[48] Elsafi AM. Exergy and exergoeconomic analysis of sustainable direct steam generation solar power plants. Energy Convers Manage 2015;103:338–47. https://doi.org/10.1016/j.enconman.2015.06.066.
[49] Starke AR, Cardemil JM, Escobar RA, Colle S. Assessing the performance of hybrid CSP + PV plants in northern Chile. Sol Energy 2016;138:88–97. https://doi.org/10.1016/j.solener.2016.09.006.
[50] Servert JF, Cerrajero E, Fuentealba EL. Synergies of Solar Energy Use in the Desalination of Seawater: a Case Study in Northern Chile. SolarPACES; 2015.